

**THE COMPOSITION OF Co–Ni–Fe SULFARSENIDES,  
DIARSENIDES AND TRIARSENIDES FROM THE SAN JUAN DE PLAN DEPOSIT,  
CENTRAL PYRENEES, SPAIN**

ISABEL FANLO<sup>§</sup> AND IGNACIO SUBÍAS

*Cristalografía y Mineralogía. Departamento de Ciencias de la Tierra.  
Universidad de Zaragoza, C/ Pedro Cerbuna 12, E–50009 Zaragoza, Spain*

FERNANDO GERVILLA

*Instituto Andaluz de Ciencias de la Tierra y Departamento de Mineralogía y Petrología.  
Facultad de Ciencias, C.S.I.C.–Universidad de Granada, E–18002 Granada, Spain*

ANDRÉS PANIAGUA AND BELÉN GARCÍA

*Cristalografía y Mineralogía. Departamento de Ciencias de la Tierra.  
Universidad de Zaragoza, C/ Pedro Cerbuna 12, E–50009 Zaragoza, Spain*

ABSTRACT

The San Juan de Plan deposit, in the central Pyrenees of Spain, is situated in an ankeritic horizon in Silurian black shales. The main association consists of pyrite, sulfarsenides, diarsenides, and Co triarsenides (skutterudite), as well as a late stage consisting of cobaltite, Fe, Cu and Bi sulfides and native Bi. The sulfarsenides are arsenopyrite, alloclasite, members of the gersdorffite–cobaltite solid-solution series, arsenic-rich gersdorffite and cobaltite, whereas the diarsenides range from rammelsbergite to safflorite. Rammelsbergite is characterized by a composition within the range  $(\text{Ni}_{0.71-0.97}\text{Co}_{0.02-0.29}\text{Fe}_{0.00-0.02})\text{As}_{1.75-2.01}\text{S}_{0.00-0.26}$ , exceeding the theoretical value  $(\text{As}_{1.93}\text{S}_{0.07})$  given by Yund (1962). Two generations of the gersdorffite–cobaltite solid-solution series have been found on the basis of textural features and chemical composition; the first,  $(\text{Co}_{0.10-0.77}\text{Ni}_{0.07-0.80}\text{Fe}_{0.03-0.58})\text{As}_{0.95-1.27}\text{S}_{0.75-1.06}$ , shows a positive correlation between S and Fe contents, and between Co and As contents, whereas the second one,  $(\text{Co}_{0.02-0.91}\text{Ni}_{0.02-0.96}\text{Fe}_{0.00-0.28})\text{As}_{0.99-1.38}\text{S}_{0.67-1.01}$ , exhibits a considerable compositional field in the Fe-poor region of the system  $\text{CoAsS–NiAsS–FeAsS}$ , providing evidence of extensive substitution of Co by Ni, with a positive correlation between As and Ni contents. Arsenic-rich gersdorffite displays a broad range of As and S mutual substitution,  $(\text{Ni}_{0.65-0.98}\text{Co}_{0.02-0.27}\text{Fe}_{0.00-0.06})\text{As}_{1.37-1.83}\text{S}_{0.22-0.64}$ , exceeding the experimental value of  $\text{NiAs}_{1.77}\text{S}_{0.23}$  reported by Yund (1962). The presence of alloclasite and the extent of the solid-solution fields of the cobaltite–gersdorffite series suggest that the main assemblage of minerals at the San Juan de Plan deposit formed at temperatures as high as 600°C. Preliminary geothermometric data obtained on graphite support such a high temperature.

*Keywords:* Ni–Co–Fe sulfarsenides, gersdorffite–cobaltite solid-solution series, alloclasite, As-rich gersdorffite, rammelsbergite, skutterudite, compositional trends, San Juan de Plan, Spain.

SOMMAIRE

Le gisement de San Juan de Plan, situé dans les Pyrénées centrales de l'Espagne, se trouve dans un couche ankéritique d'une séquence de shales noirs d'âge silurien. Le minerai est fait surtout de pyrite, de sulfarséniures, de diarséniures et de triarséniures de cobalt (skutterudite), de même que de cobaltite, de sulfures de Fe, Cu et Bi, et de bismuth natif, déposés tardivement. Parmi les sulfarséniures se trouvent arsénopyrite, alloclasite, des membres de la solution solide gersdorffite–cobaltite, la gersdorffite et la cobaltite enrichies en arsenic, tandis que les diarséniures vont de la rammelsbergite à la safflorite. La rammelsbergite possède une composition dans l'intervalle  $(\text{Ni}_{0.71-0.97}\text{Co}_{0.02-0.29}\text{Fe}_{0.00-0.02})\text{As}_{1.75-2.01}\text{S}_{0.00-0.26}$ , et dépasse ainsi la valeur théorique attribuée par Yund (1962),  $(\text{As}_{1.93}\text{S}_{0.07})$ . Nous avons trouvé deux générations de compositions faisant partie de la série gersdorffite–cobaltite, comme en témoignent les attributs texturaux et la composition chimique; la première,  $(\text{Co}_{0.10-0.77}\text{Ni}_{0.07-0.80}\text{Fe}_{0.03-0.58})\text{As}_{0.95-1.27}\text{S}_{0.75-1.06}$ , fait preuve d'une corrélation positive entre les teneurs en S et Fe, et en Co et As, tandis que la seconde,  $(\text{Co}_{0.02-0.91}\text{Ni}_{0.02-0.96}\text{Fe}_{0.00-0.28})\text{As}_{0.99-1.38}\text{S}_{0.67-1.01}$ , exhibe un champ compositionnel considérable dans la région pauvre en Fe du système  $\text{CoAsS–NiAsS–FeAsS}$ , fournissant des preuves d'une substitution étendue de Co par Ni, avec une corrélation positive entre As et Ni. La gersdorffite riche en arsenic présente une large gamme de substitution mutuelle de As et S,  $(\text{Ni}_{0.65-0.98}\text{Co}_{0.02-0.27}\text{Fe}_{0.00-0.06})\text{As}_{1.37-1.83}\text{S}_{0.22-0.64}$ , dépassant la valeur expérimentale de  $\text{NiAs}_{1.77}\text{S}_{0.23}$  rapportée par Yund (1962). La présence d'alloclasite et l'étendue des champs de solution solide de la série gersdorffite–cobaltite suggèrent que l'assemblage principal de minéraux au gisement de San Juan de Plan s'est formé à des températures aussi élevées que 600°C. Des données géothermométriques préliminaires obtenues sur du graphite soutiennent une telle température élevée.

<sup>§</sup> E-mail address: fanlo@unizar.es

$_{0.91}\text{Ni}_{0.02-0.96}\text{Fe}_{0.00-0.28}\text{As}_{0.99-1.38}\text{S}_{0.67-1.01}$ , possède une étendue considérable du champ de compositions dans la région pauvre en Fe du système  $\text{CoAsS-NiAsS-FeAsS}$ , montrant ainsi un remplacement important du Co pour le Ni, avec une corrélation positive entre les teneurs en As et en Ni. La gersdorffite riche en arsenic montre en fait une variabilité importante de As et de S, sur l'intervalle  $(\text{Ni}_{0.65-0.98}\text{Co}_{0.02-0.27}\text{Fe}_{0.00-0.06})\text{As}_{1.37-1.83}\text{S}_{0.22-0.64}$ , dépassant ainsi la valeur expérimentale proposée par Yund (1962),  $\text{NiAs}_{1.77}\text{S}_{0.23}$ . La présence de l'allosite et l'étendue du phénomène de solutions solides des séries cobaltite-gersdorffite font penser que l'assemblage principal des minéraux du gisement de San Juan de Plan s'est formé à une température élevée, possiblement 600°C. Des données géothermométriques préliminaires fondées sur le graphite concordent avec une telle température élevée.

(Traduit par la Rédaction)

**Mots-clés:** sulfarsénures de Ni-Co-Fe, solution solide gersdorffite-cobaltite, allosite, gersdorffite riche en arsenic, rammelsbergite, skutterudite, tracés de composition, San Juan de Plan, Espagne.

## INTRODUCTION

We present here a detailed mineralogical and microanalytical study of sulfarsenides, diarsenides and triarsenides from the San Juan de Plan deposit, central Pyrenees, Spain. We wish to establish the different paragenetic assemblages in order to understand the evolution of the ore-forming process. These assemblages include, among other sulfarsenides and diarsenides, allosite, members of the gersdorffite-cobaltite solid-solution series, and As-rich gersdorffite coexisting with rammelsbergite. According to the experimental results of Yund (1962), Klemm (1965b), Maurel & Picot (1974) and Hem & Makovicky (2004), these assemblages must have formed at temperatures above 650–600°C.

## BACKGROUND INFORMATION

Compositional data reported in the literature, experimental determinations and theoretical considerations on phase relations in the system  $\text{Co-Ni-Fe-As-S}$  indicate the existence of the following features. 1) There is complete miscibility between gersdorffite ( $\text{NiAsS}$ ) and cobaltite ( $\text{CoAsS}$ ) above 550°C. Conversely, the miscibility between arsenopyrite ( $\text{FeAsS}$ ) and gersdorffite-cobaltite solid-solution series is limited. The solvus reported by Klemm (1965b) in the system  $\text{CoAsS-NiAsS-FeAsS}$  at temperatures between 650° and 300°C has been used as a geothermometric indicator (e.g., Misra & Fleet 1975, Oen *et al.* 1984, Gervilla & Rønso 1992, Gervilla *et al.* 1996, 1998, Hem *et al.* 2001), in some cases yielding contradictory temperatures. 2) Limited miscibility exists between gersdorffite (cubic phase) and rammelsbergite (orthorhombic phase,  $\text{NiAs}_2$ ) along the rammelsbergite-vaesite ( $\text{NiS}_2$ ) join. According to Yund (1962), the maximum As content of gersdorffite corresponds to the formula  $\text{NiAs}_{1.77}\text{S}_{0.23}$ , and the maximum S content of rammelsbergite is  $1.1 \pm 0.1$  wt% at 700°C. Nevertheless, a complete range of compositions between gersdorffite ( $\text{NiAsS}$ ) and krutovite (cubic phase,  $\text{NiAs}_2$ ) has been reported by Spiridonov & Chvileva (1995). 3) There is a small but real deficiency in arsenic in synthetic skutterudite, which also exists in

natural skutterudite (Roseboom 1962, Nickel 1970). Recently, Hem & Makovicky (2004) have reported synthetic skutterudite with a *Me:X* ratio from 1:2.84 to 1:3.02.

Hem & Makovicky (2004) investigated the phase relations in the As-rich regions of the  $(\text{Fe,Ni,Co})(\text{As,S})_2$  prism at 650° and 500°C. They found that most of the phases exhibit extensive solid-solution at 650°C, both in the systems  $\text{Fe-Ni-Co}$  and  $\text{As-S}$ . These authors confirmed the existence of complete solid-solution between gersdorffite and cobaltite at 650°C and showed the existence of complete solid-solutions among safflorite, allosite  $[(\text{Co,Fe})\text{AsS}]$ , skutterudite and their respective  $(\text{Fe}_{0.5}\text{Ni}_{0.5})$  analogues. However, these solid-solutions are more restricted with respect to  $\text{Fe-Co-Ni}$  at 500°C, but they still show a large variation in  $\text{As-S}$ . They also found a nickel diarsenide containing up to 1 at.% Co or Fe and 12–14 at.% S coexisting with gersdorffite. This phase, formed at 650° and 500°C, was identified as krutovite ( $\text{NiAs}_2$ ). The phase in question contains much more sulfur than rammelsbergite formed at 600° and 700°C, as determined by Yund (1962). Krutovite formed at 500°C is notably richer in As than at 650°C and also coexists with gersdorffite. By powder X-ray diffraction (PXRD) and least-squares refinement of the unit cells of (Fe,Co)-free gersdorffite and krutovite, Hem & Makovicky (2004) gave the space group *Pa3*, with *a* equal to 5.6917 Å for gersdorffite and 5.723 Å for the coexisting krutovite. This krutovite has compositions that partially overlap the gersdorffite field, as described by Yund (1962).

## THE SAN JUAN DE PLAN DEPOSIT

Mining activities in the San Juan de Plan area were first recorded in 1730 and concentrated on the cobalt ores. During the major period of mining activity from 1830 to 1870, 35 t/yr were extracted with Co and Ni grades of 11 and 7%, respectively. Since then, mining operations have been carried out at various scales. The last period of cobalt production ended in 1936. Later attempts to discover new resources failed.

The ore is enclosed in a carbonate horizon at the top of a sequence of Silurian black shales. The roughly stratiform ore-bearing unit is 500 m long, with a maximum thickness of 2 m, and is extensively converted to ankerite. The origin of this ankerite is epigenetic (Castroviejo & Nodal 1985), on the basis of contact relationships between the ankerite and the precursor Silurian limestones. The ore-bearing ankerite horizon is controlled by east–west fractures and is located beneath Triassic red beds, which were deposited at the top of an erosional surface affecting the Paleozoic basement. This basement comprises a monotonous detrital sequence referred to as Cambrian–Ordovician, pre-Variscan augen gneisses and granitic gneisses, a Devonian sequence made up of limestones, calcareous slates and slates, and Carboniferous rocks composed of cherts, nodular limestones, dark slates and turbiditic sandstones. Granodioritic batholiths intrude the Paleozoic rocks. In places, ore deposits are hosted by porphyritic granitic dykes, which were emplaced along east–west fractures and the schistosity planes in black shales. The hydrothermal fluids promoted alteration of the dyke rocks (white mica and chlorite), the conversion of limestones to ankerite, and mineralization of replaced units.

Ore minerals typically occur as decimetric pockets, disseminations and veinlets locally linked to stylolitic seams rich in organic matter. Microscopic examinations confirm that the ore minerals are contemporaneous or rarely postdate ankerite formation. The ankerite and the ore minerals thus originated from the same process.

#### MINERALOGY AND PETROGRAPHY

Mineral assemblages found in the San Juan de Plan deposit contain Co–Ni–Fe sulfarsenides, diarsenides and triarsenides, along with pyrite, arsenopyrite, nickeline, chalcopyrite, marcasite, native bismuth and bismuthinite. The gangue minerals mostly consist of ankerite, dolomite, and calcite. The more significant textural features of the San Juan de Plan deposit are replacements and overgrowths, as evidenced by large variations in Fe–Co–Ni and As–S proportions in the zoned sulfarsenides.

Six stages of mineral deposition can be distinguished on the basis of the mineral association: Stage I: pyrite I, arsenopyrite, and scarce nickeline; Stage II: Co triarsenides (skutterudite I), and diarsenides (safflorite); Stage III: Co–Ni–Fe sulfarsenides: alloclasite and gersdorffite–cobaltite solid solution ( $GC_{ss}$  I); Stage IV: Ni–Co sulfarsenides: gersdorffite–cobaltite solid solution ( $GC_{ss}$  II), arsenic-rich gersdorffite (As–Gdf) and Ni diarsenides (rammelsbergite and krutovite?); Stage V: Co triarsenides (skutterudite II); Stage VI: cobaltite, bismuthinite, pyrite II, chalcopyrite, marcasite and native bismuth (Fig. 1).

Stage I consists of euhedral pyrite I and arsenopyrite. Pyrite crystals are fractured and brecciated along cleavages. Locally, pyrite crystals act as nuclei for the crystallization of zoned  $GC_{ss}$  I and As–Gdf crystals at

the outer rim (Fig. 2A). Arsenopyrite occurs as discrete euhedral crystals, in some cases replaced by one or both generations of  $GC_{ss}$  crystals or alloclasite masses (Fig. 2B). No zoned, hourglass or obvious disequilibrium textures were observed in the arsenopyrite. This stage closes with the crystallization of nickeline, which has only been found as remnants of resorption in skutterudite I (Fig. 2C).

Stage II is marked by a drop in sulfur fugacity and a strong increase in arsenic fugacity, corresponding to the crystallization of triarsenides and diarsenides of cobalt. Skutterudite I is a scarce mineral; it occurs as minute inclusions in  $GC_{ss}$  II and As–Gdf crystals (Fig. 2C), and as irregular masses or euhedral crystals partially replaced by alloclasite (Fig. 2D). Safflorite also is scarce; it occurs as small and irregular masses enclosed in and partly replaced by alloclasite or  $GC_{ss}$  I crystals (Fig. 2E).

During stage III, sulfur fugacity increased slightly (and arsenic fugacity decreased), as deduced from the crystallization of alloclasite and  $GC_{ss}$  I. Alloclasite exhibits clear purple to mauve to greenish olive rotation tints and occurs as skeletal masses or, locally, as rhomb-shaped crystals (Fig. 2D). The alloclasite areas contain well-defined optical sectors with lamellae parallel to crystals faces. Some irregular masses of alloclasite enclose euhedral crystals of pyrite I and arsenopyrite.  $GC_{ss}$  I crystals are present as skeletal and irregular masses, euhedral to subhedral single crystals, or massive aggregates. The skeletal and irregular masses partially replace alloclasite (Fig. 2E) and rhombs of arsenopyrite.

Stage IV is characterized by the simultaneous deposition of gersdorffite–cobaltite solid-solution series ( $GC_{ss}$  II) and arsenic-rich gersdorffite (As–Gdf). In fact,  $GC_{ss}$  II overgrows As–Gdf crystals showing idiomorphic terminations (Fig. 2F) or *vice versa*; the idiomorphic  $GC_{ss}$  II crystals, showing significant growth-induced zoning, very fine in scale, of regular thickness and showing small variations in the As:S ratio and Ni contents, are overgrown by As–Gdf crystals (Figs. 2C, G). In addition, As–Gdf, or locally  $GC_{ss}$  II, overgrew (Figs. 2H, I) irregular patches or euhedral lath-shaped crystals of  $GC_{ss}$  I, and replaced and filled small cracks in these crystals. Arsenic-rich gersdorffite (As–Gdf) is not invariably a homogeneous phase, as the crystals show irregular microscopic growth-bands (Fig. 2G) characterized by small variations in the As and S contents but with no variation in metal content. Likewise, transitions between  $GC_{ss}$  I and  $GC_{ss}$  II and between these latter minerals and As–Gdf crystals have been recognized. Stage IV ends with the crystallization of rammelsbergite, which exhibits complex twinning consisting of extremely fine lamellae, with at least two twin laws, and rotation tints rich in different shades of blue, which indicates that rammelsbergite may come from pre-existing cubic krutovite. Rammelsbergite shows various modes of occurrence: (1) aggregates of prismatic tabular grains, randomly oriented with typical polysynthetic twins and, in some cases, enclosing

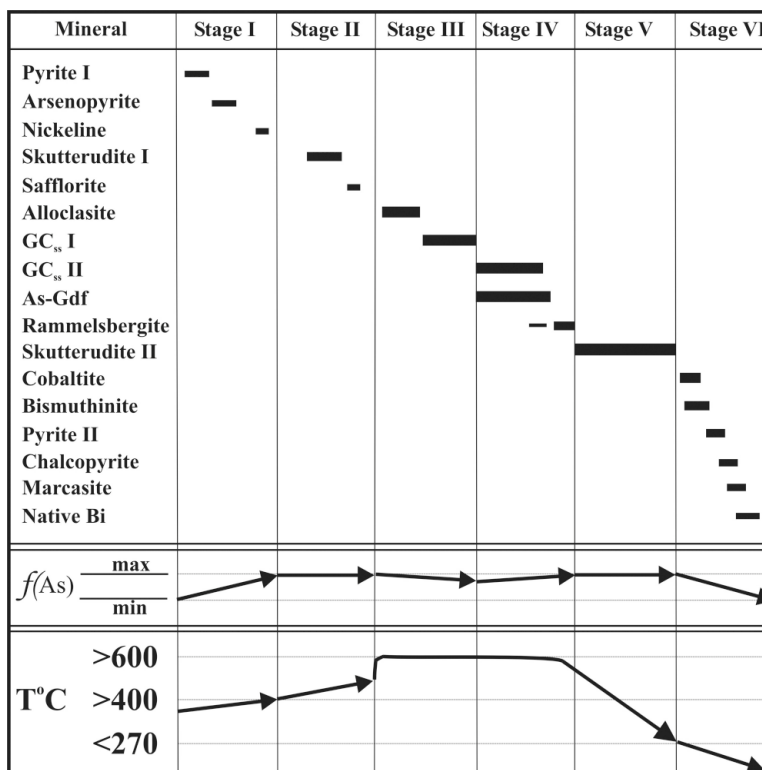


FIG. 1. Paragenetic sequence of the mineralization at San Juan de Plan. The estimated fugacity of arsenic and temperature during the precipitation of the different stages are shown. GC<sub>ss</sub> I, II: gersdorffite–cobaltite solid-solution series; As–Gdf: arsenic-rich gersdorffite.

ehedral crystals of skutterudite I, (2) skeletal masses, or small lath-shaped crystals with parallel alignment or pods in coarse idiomorphic crystals of skutterudite II (Figs. 2J, K), and (3) euhedral to subhedral single crystals partially replaced by crystals of skutterudite II.

Stage V represents a further increase in the activity of arsenic, as indicated by the crystallization of skutterudite II. This mineral occurs as idiomorphic crystals replacing or overgrowing GC<sub>ss</sub> II, rammelsbergite and arsenic-rich gersdorffite (As–Gdf) crystals, which can be seen as islands along crystallographic directions in skutterudite II (Figs. 2J, K). Etching with HNO<sub>3</sub> revealed zoning in skutterudite II without relation to compositional changes.

The mineral assemblage formed during stage VI consists of cobaltite, bismuthinite, pyrite II, native bismuth, chalcopyrite and marcasite. It shows characteristic textures of crystal growth in open spaces. Cobaltite precipitation is associated with bismuthinite and shows two distinctly different modes of occurrence: (1) subhedral grains isolated or forming aggregates of small

size, with numerous micro-faults filled by bismuthinite; in some cases, both minerals show sharp contacts, which may suggest contemporaneous crystallization, and (2) irregular and small masses replacing both GC<sub>ss</sub> II and As–Gdf crystals (Fig. 2F). Chalcopyrite fills cracks in skutterudite II, encloses GC<sub>ss</sub> I masses or where associated with bismuthinite, fills open spaces among GC<sub>ss</sub> II idiomorphic crystals. Pyrite II is partially transformed to marcasite and fills fractures and interstices in the mineral assemblage. Native bismuth is found as small inclusions within the earlier minerals or, as irregular masses filling the interstices and open spaces between rammelsbergite and skutterudite II.

#### MINERAL COMPOSITIONS

Most of the samples investigated in this study were obtained from the Asociación Mineralógica Aragonesa Museum and private collections; additional material was collected from dumps and accessible galleries. Thirty samples were studied by reflected-light microscopy,

electron probe microanalysis, and X-ray diffraction using the powder method (PXRD).

Chemical compositions of the minerals investigated were determined by wavelength-dispersion electron-probe micro-analysis using a CAMECA SX-50 instrument at the University of Barcelona. The opaque minerals were analyzed for Fe, Co, Ni, As and S; Sb, Cu, Bi, Zn, Pt and Pd were found to be below the detection limit or not detected. We monitored the peaks due to FeK $\alpha$ , CoK $\alpha$ , NiK $\alpha$ , SK $\alpha$ , AsL $\alpha$ , SbL $\alpha$ , CuK $\alpha$ , ZnK $\alpha$ , BiL $\alpha$ , and PbM $\alpha$ . Operating conditions included an accelerating voltage of 20 kV and a beam current of 20 nA. The counting times were 20 s on TAP/PET and 30 s on LiF crystals. The ZAF corrections were performed using the program supplied by CAMECA. Pyrite, GaAs, NiO, as well as pure Co metal, were used as primary standards. The maximum, minimum, mean and representative results of point analyses are given below in tables.

#### Pyrite and arsenopyrite

Pyrite has a nearly stoichiometric composition (Table 1): only minor As, Co and Ni contents were detected. Arsenopyrite (Table 1) contains some cobalt (up to 2.13 wt%), but no nickel or antimony. The composition varies over the range (Fe<sub>0.94–1.02</sub>Co<sub>0.00–0.06</sub>)As<sub>0.88–1.01</sub>S<sub>0.99–1.11</sub>.

#### Skutterudite

Two generations of skutterudite can be distinguished on the basis of textural criteria (Fig. 1) and chemical composition (Table 2). Skutterudite I (stage II, Figs. 2C, D) is characterized by low Ni contents and the absence of Fe [(Co<sub>0.89–0.99</sub>Ni<sub>0.00–0.11</sub>)As<sub>2.84–2.99</sub>S<sub>0.03–0.17</sub>], whereas skutterudite II (stage V, Fig. 2J) is marked by a broader range of compositions [(Co<sub>0.50–0.90</sub>Fe<sub>0.05–0.22</sub>Ni<sub>0.05–</sub>

<sub>0.45</sub>)As<sub>2.75–3.01</sub>S<sub>0.00–0.24</sub>]. Skutterudite II shows a substantial replacement of Co by Ni and Fe, in the range of 1.35–11.35 at.% Ni and 1.36–5.59 at.% Fe, and a limited replacement of As by S (0.00 to 6.12 at.% S), but definitely higher than skutterudite I (from 0.70 to 4.14 at.% S). In both generations of skutterudite, As is negatively correlated with S (R = –0.97), whereas Ni and Fe show a weak positive correlation with As.

The compositions of skutterudite I and II plot within the solid-solution field (shaded area) defined by Roseboom (1962), Klemm (1965a) and Rosner (1970) in Co–Ni–Fe space (Fig. 3A). The arrows in Figure 3A show the compositional trends exhibited by the aforementioned generations of skutterudite. In skutterudite I, Co is replaced by Ni (Ni trend), whereas Co is replaced by a mixture of Ni and Fe (Ni/Fe trend) in skutterudite II. The regression line describing the composition of skutterudite II is Ni = 0.65346 – 0.65319 (Co + Fe), with R = 0.801. The Ni/Fe trend begins in the Co corner and cuts the Ni–Fe join at Ni<sub>0.65</sub>Fe<sub>0.35</sub>.

In addition, the As–S plot (Fig. 3B), with a regression line of As = 2.99699 – 0.96198 S, R = 0.969) reveals that a significant part of the analyzed skutterudite does not show a deficiency in As (note that although only two points are over the y-axis indicating S = 0 and As = 3.0 atoms per formula unit, *apfu*, they actually are representing 15 points). These analytical results constitute a discrepancy with the experimental work of Roseboom (1962), who said that natural skutterudite has a deficiency in arsenic.

#### Diarsenides

Electron-microprobe analyses show that safflorite has a nearly stoichiometric composition (Table 3): (Co<sub>0.89–0.97</sub>Fe<sub>0.02–0.10</sub>Ni<sub>0.00–0.02</sub>)As<sub>1.85–1.97</sub>S<sub>0.04–0.16</sub>, and that As content is negatively correlated with S content. The regression line describing the relation between As

TABLE 1. STATISTICAL RESULTS OF ELECTRON-MICROPROBE ANALYSES OF PYRITE AND ARSENOPIRYTE FROM THE SAN JUAN DE PLAN DEPOSIT, CENTRAL PYRENEES, SPAIN

		Compositions (weight %)						Atoms per formula unit					
		S	As	Fe	Co	Ni	Total	S	As	Fe	Co	Ni	As#
Py <i>n</i> = 27	min	50.95	0.01	44.70	0.04	n.d.	99.25	1.95	0.00	0.98	0.00	0.00	-
	max	53.41	1.70	47.69	1.10	0.39	100.30	2.01	0.02	1.03	0.02	0.01	-
	mean	52.58	0.28	46.30	0.16	0.10	99.79	1.99	0.00	1.01	0.00	0.00	-
	C118	53.01	0.07	46.25	0.17	0.25	99.30	1.99	0.00	1.00	0.00	0.00	-
Apy <i>n</i> = 17	min	19.09	41.23	33.08	0.02	n.d.	98.80	0.99	0.88	0.94	0.00	0.00	0.44
	max	22.39	45.80	35.42	2.13	0.28	100.29	1.11	1.01	1.02	0.06	0.00	0.51
	mean	21.36	42.81	34.64	0.34	0.08	99.65	1.07	0.92	1.00	0.01	0.00	0.46
	32	22.04	41.23	34.73	0.18	0.11	99.11	1.11	0.89	1.00	0.00	0.00	0.45
	35	22.20	41.86	35.10	0.39	0.07	100.29	1.11	0.89	0.99	0.02	0.00	0.44
	37	21.27	43.52	35.03	0.07	0.02	100.20	1.06	0.93	1.01	0.00	0.00	0.47
	38	21.87	42.48	35.42	0.02	0.04	99.96	1.09	0.91	1.01	0.00	0.00	0.46

Representative results of micro-analyses are indicated in Figures 2A and 2B, respectively. As#: As/(As + S).

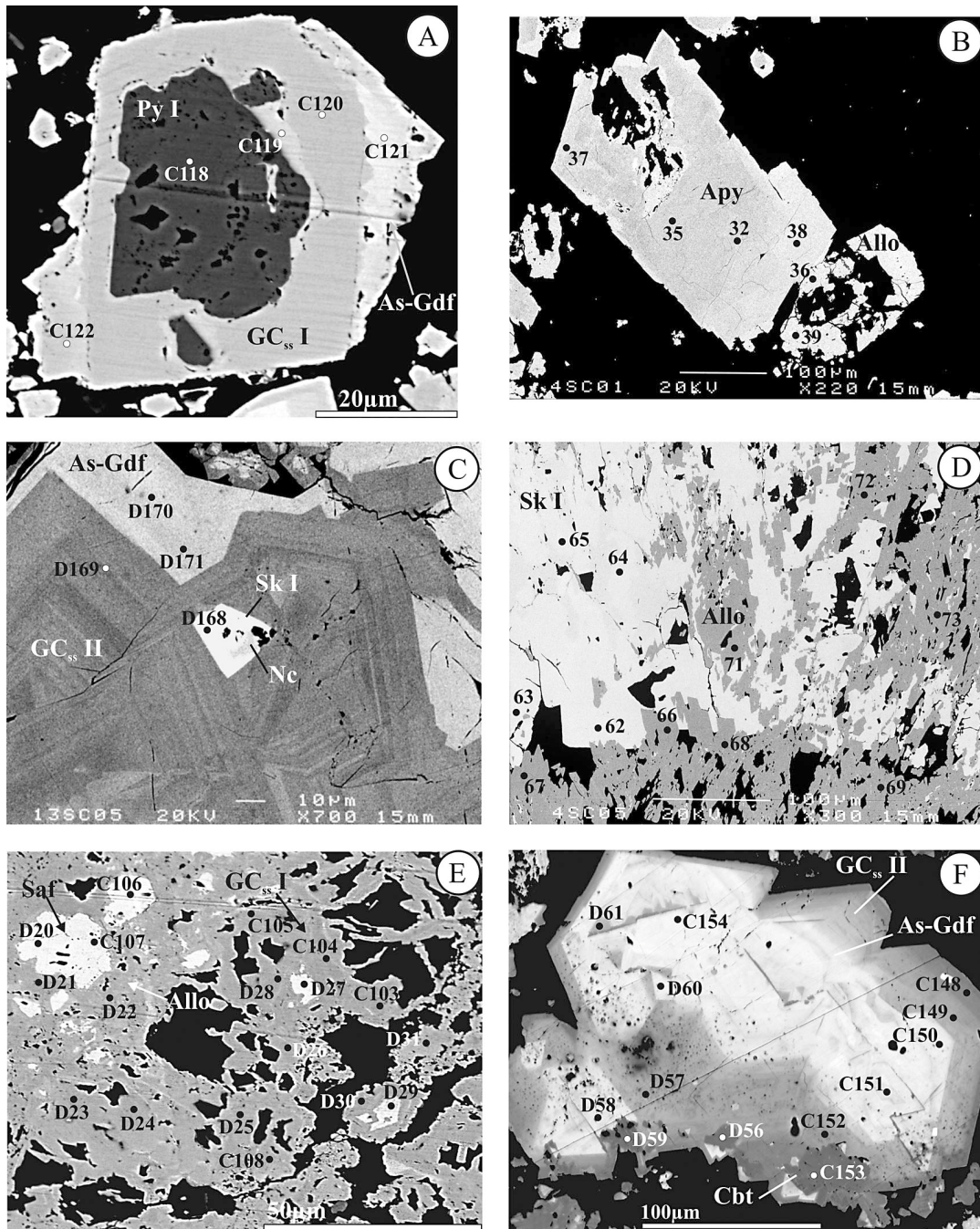
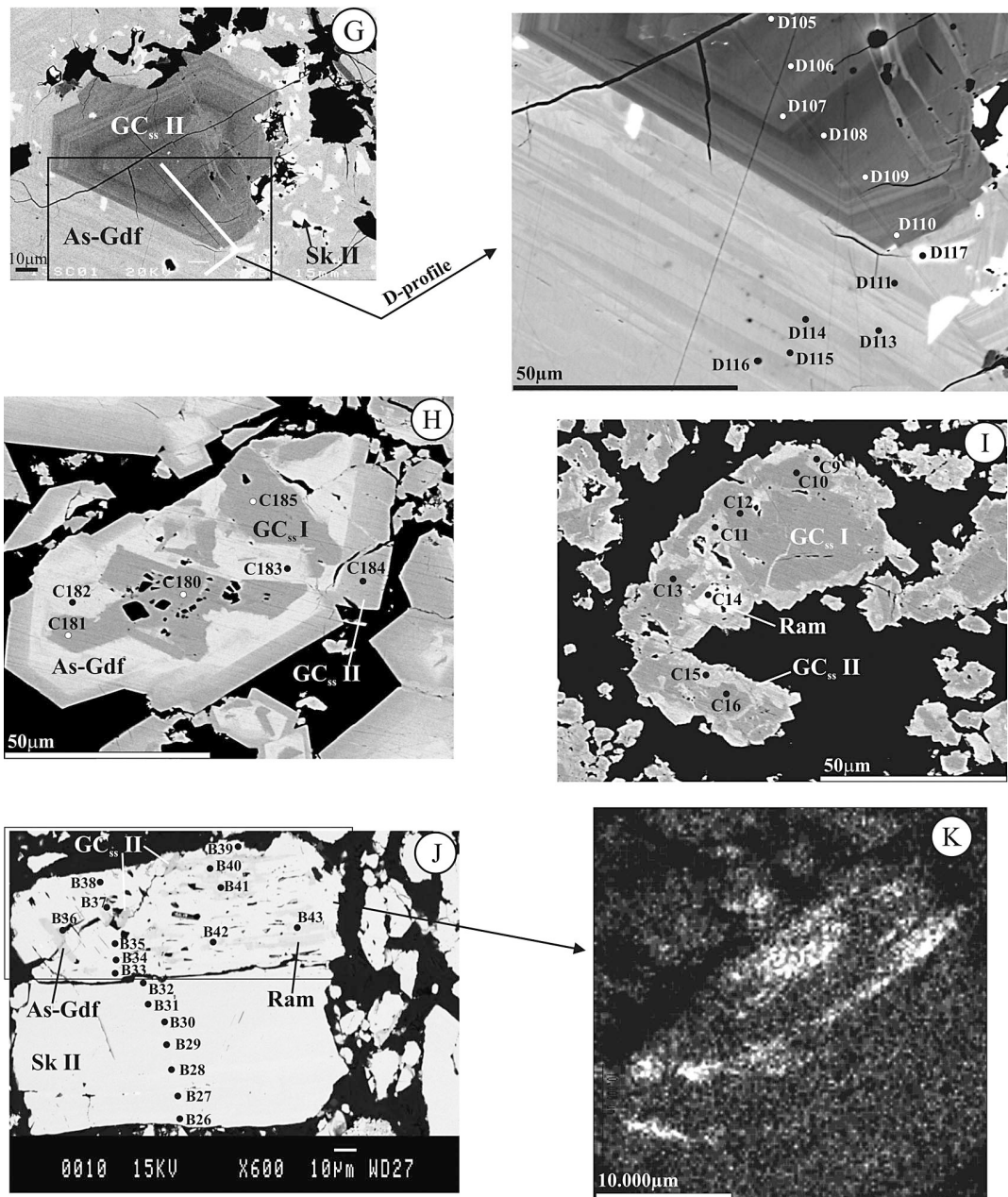


FIG. 2. Back-scattered electron images showing representative textures of the San Juan de Plan deposit. The numbers indicate compositions referenced in Tables 1 to 6. Symbols: Py I: pyrite from stage I; Apy: arsenopyrite; Nic: nickeline; Sk I: skutterudite from stage II; Sk II: skutterudite from stage V; Saf: safflorite; Ram: rammelsbergite; Allo: alloclasite; GC<sub>ss</sub> I: gersdorffite-cobaltite solid-solution from stage III; GC<sub>ss</sub> II: gersdorffite-cobaltite solid-solution from stage IV; As-Gdf: arsenic-rich gersdorffite; Cbt: cobaltite from stage VI. (A). Pyrite I (Py I) enclosed by GC<sub>ss</sub> I and As-Gdf crystals. (B). Euhedral crystal of arsenopyrite (Apy) partially replaced by alloclasite (Allo). (C). Minute inclusion of nickeline (Nc) hosted by skutterudite I (Sk I), which, in turn, is overgrown by GC<sub>ss</sub> II, showing complex zoning and growth history. The overgrowth



is composed of As–Gdf. (D). Alloclastic (Allo) replaces skutterudite I (Sk I) showing rhomb-shaped crystals. (E). Skeletal masses of safflorite (Saf) being replaced by alloclastic (Allo) or GC<sub>ss</sub> I. (F). Idiomorphic crystal of As–Gdf, partially replaced and overgrown by GC<sub>ss</sub> II, which displays oscillatory growth-zonation. Both minerals are replaced by cobaltite (Cbt). (G). Idiomorphic crystals of GC<sub>ss</sub> II showing very fine oscillatory growth-zonation, perfectly overgrown by As–Gdf, which shows irregular zonation; skutterudite II (Sk II) fills open spaces and partly replaces both minerals. (H). Irregular patches or lath-shaped crystal of GC<sub>ss</sub> I overgrown by As–Gdf, which is, in turn, overgrown by GC<sub>ss</sub> II. (I). Small crystals of rammelsbergite (Ram) and irregular masses of GC<sub>ss</sub> I hosted by GC<sub>ss</sub> II. Note that GC<sub>ss</sub> II also fills cracks affecting GC<sub>ss</sub> I. (J). Idiomorphic skutterudite II (Sk II) replaces or overgrows GC<sub>ss</sub> II, As–Gdf and rammelsbergite (Ram), which can be seen as islands along the crystallographic directions. (K). NiK $\alpha$  X-ray image of the top of the Figure 2J showing the location of As–Gdf and rammelsbergite crystals; the photomicrograph is rotated 30° with respect to Figure 2J.

TABLE 2. STATISTICAL RESULTS OF ELECTRON-MICROPROBE ANALYSES OF SKUTTERUDITE I (STAGE II) AND SKUTTERUDITE II (STAGE V) FROM THE SAN JUAN DE PLAN DEPOSIT, CENTRAL PYRENEES, SPAIN

		Compositions (weight %)						Atoms per formula unit					
		S	As	Fe	Co	Ni	Total	S	As	Fe	Co	Ni	As#
Sk I n = 7	min	0.21	77.25	0.08	19.00	0.25	101.07	0.03	2.84	0.00	0.89	0.00	0.94
	max	1.9	79.86	0.27	20.92	2.42	101.62	0.17	2.99	0.00	0.99	0.11	0.99
	mean	0.88	78.68	0.13	20.13	1.05	101.22	0.08	2.93	0.00	0.95	0.04	0.97
	D168	0.51	79.35	0.09	19.00	2.42	101.35	0.06	2.94	0.00	0.89	0.11	0.98
	62	1.41	78.00	0.10	20.90	0.66	101.30	0.11	2.89	0.00	0.97	0.03	0.96
	63	0.62	78.80	0.17	20.70	0.25	101.17	0.06	2.96	0.00	0.99	0.00	0.98
	64	1.90	77.25	0.27	20.73	0.61	101.62	0.17	2.84	0.00	0.97	0.03	0.94
	65	1.13	78.20	0.14	20.90	0.26	101.03	0.11	2.91	0.00	0.98	0.00	0.96
Sk II n = 84	min	0.03	75.87	0.84	10.50	0.89	99.39	0.00	2.75	0.05	0.50	0.05	0.92
	max	2.84	80.14	4.52	19.74	9.21	102.19	0.24	3.01	0.22	0.90	0.45	1.00
	mean	1.02	78.32	2.25	14.30	4.41	100.60	0.09	2.91	0.11	0.68	0.21	0.97
	D117	0.52	79.24	2.24	15.98	2.89	100.99	0.06	2.94	0.11	0.75	0.14	0.98
	B26	2.24	76.6	1.15	16.67	3.54	100.47	0.19	2.81	0.06	0.77	0.17	0.94
	B27	1.79	77.16	0.84	15.31	5.05	100.29	0.16	2.82	0.05	0.71	0.25	0.95
	B28	2.09	76.75	1.40	16.13	3.86	100.30	0.19	2.79	0.08	0.74	0.19	0.94
	B29	1.18	78.05	2.82	14.40	3.91	100.45	0.11	2.89	0.14	0.67	0.19	0.96
	B30	1.80	77.22	1.59	15.48	3.92	100.16	0.17	2.84	0.08	0.72	0.19	0.94
	B31	1.27	77.87	1.38	14.31	5.54	100.69	0.11	2.91	0.06	0.67	0.25	0.96
	B32	1.30	77.48	1.54	15.64	3.65	99.75	0.11	2.88	0.08	0.76	0.17	0.96
	B33	1.26	77.81	0.89	14.38	5.57	100.22	0.11	2.91	0.06	0.67	0.25	0.96
	B34	0.11	79.59	2.71	13.15	4.84	100.56	0.00	3.01	0.14	0.62	0.23	1.00
	B35	0.07	79.66	2.46	13.69	4.52	100.71	0.00	3.01	0.11	0.65	0.23	1.00
	B38	0.05	79.55	3.66	12.03	5.22	100.66	0.00	2.99	0.02	0.56	0.25	1.00
	B39	0.97	78.24	1.81	12.71	6.62	100.40	0.08	2.91	0.08	0.62	0.31	0.97

Representative results of micro-analyses are indicated in Figures 2D, 2G, and 2J. As#: As/(As + S).

TABLE 3. STATISTICAL RESULTS OF ELECTRON-MICROPROBE ANALYSES OF SAFFLORITE (STAGE II) AND RAMMELSBERGITE (STAGE IV) FROM THE SAN JUAN DE PLAN DEPOSIT, CENTRAL PYRENEES, SPAIN

		Compositions (weight %)						Atoms per formula unit					
		S	As	Fe	Co	Ni	Total	S	As	Fe	Co	Ni	As#
Saf n = 6	min	0.68	68.69	0.42	25.69	0.00	99.12	0.04	1.85	0.02	0.89	0.00	0.92
	max	2.44	71.13	2.97	27.96	0.71	101.68	0.16	1.97	0.10	0.97	0.02	0.98
	mean	1.77	69.62	1.47	27.11	0.35	100.50	0.11	1.89	0.05	0.93	0.01	0.95
	C106	1.99	69.84	1.44	27.47	0.57	101.63	0.12	1.86	0.06	0.94	0.02	0.94
	C107	1.47	69.65	0.95	27.66	0.48	101.11	0.10	1.89	0.04	0.95	0.02	0.95
	D20	2.44	68.83	1.13	27.96	0.00	99.12	0.16	1.85	0.04	0.95	0.00	0.92
	D27	1.70	69.67	0.42	27.69	0.00	99.84	0.10	1.91	0.02	0.97	0.00	0.95
	D29	2.34	68.69	2.97	25.69	0.35	100.36	0.14	1.85	0.10	0.89	0.02	0.93
Ram n = 42	min	0.08	66.30	0.01	0.73	19.73	99.11	0.00	1.75	0.00	0.02	0.71	0.87
	max	4.22	72.31	0.61	8.41	28.70	101.59	0.26	2.01	0.02	0.29	0.96	1.00
	mean	1.96	69.65	0.17	2.34	26.03	100.4	0.12	1.89	0.00	0.08	0.90	0.94
	C14	2.17	68.96	0.59	0.76	26.70	99.28	0.14	1.88	0.02	0.02	0.94	0.93
	B37	2.85	68.95	0.45	1.82	25.80	99.97	0.18	1.85	0.02	0.06	0.89	0.92
	B41	2.53	68.63	0.13	2.45	26.00	99.93	0.16	1.86	0.00	0.08	0.89	0.92
	B42	4.06	66.28	0.21	1.97	26.73	99.44	0.26	1.76	0.00	0.06	0.92	0.87
B43	2.90	69.36	0.40	4.37	22.68	99.81	0.18	1.87	0.02	0.14	0.79	0.91	

Representative results of micro-analyses are indicated in Figures 2D, 2I, and 2J. As#: As/(As + S).

and S is  $As = 2.008 - 1.081 S$  ( $R = -0.96$ ). Fe and Ni contents are negatively correlated with Co content ( $R = -0.94$  and  $-0.66$ , respectively). The composition of the pure cobalt end-member in the system  $CoAs_2-NiAs_2-FeAs_2$  (Fig. 4) has only been reported previously in natural assemblages by Radcliffe & Berry (1968).

Regarding rammelsbergite, the electron-microprobe data (Table 3) show a composition within the range  $(Ni_{0.71-0.96}Co_{0.02-0.29}Fe_{0.00-0.02})As_{1.75-2.01}S_{0.00-0.26}$ . There is a strong negative correlation between As and S, with a regression line  $As = 2.005 - 0.058 S$  ( $R = -0.99$ ).

## Sulfarsenides

Sulfarsenides, including alloclasite, members of the gersdorffite–cobaltite solid-solution series, arsenic-rich gersdorffite and cobaltite, are the most abundant ore minerals and were formed during stage III and stage IV, except for cobaltite, which was precipitated in stage VI (Fig. 1). The electron-microprobe data show that the compositional variability of alloclasite, expressed as  $(\text{Co}_{0.52-0.96}\text{Ni}_{0.00-0.27}\text{Fe}_{0.02-0.39})\text{As}_{0.99-1.14}\text{S}_{0.88-1.02}$ , exhibits a well-defined trend (Fig. 5A) characterized by the substitution of Co by a mixture of Ni and Fe (Table 4). According to Hem *et al.* (2001), this Ni/Fe trend is indicative of a metal-rich genetic environment. The As:S ratio ranges from 0.98 to 1.30 ( $1.07 \pm 0.06$ ),

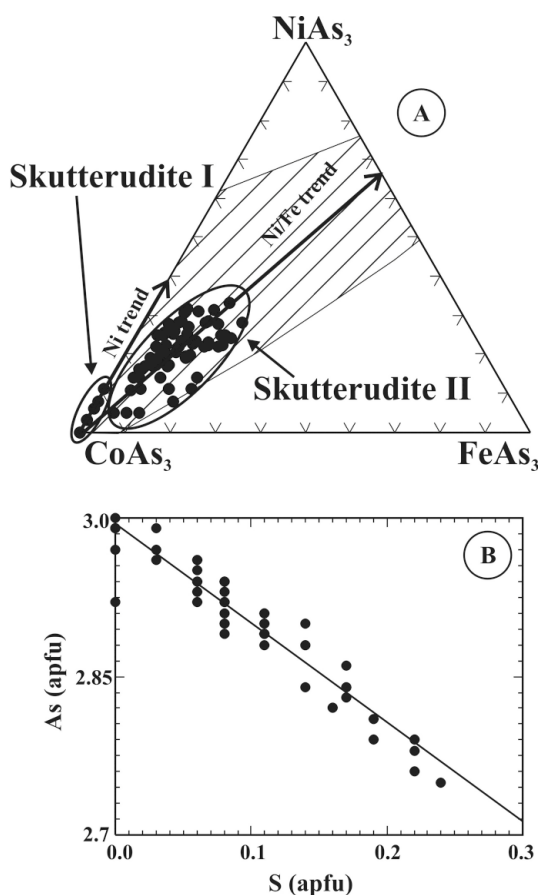


FIG. 3. A. Plot of skutterudite I and skutterudite II compositions (in mol.%) in the system  $\text{FeAs}_3\text{--CoAs}_3\text{--NiAs}_3$ . The arrows indicate the trend for each type of skutterudite, and the shaded area represents the solid-solution field defined by Roseboom (1962). B. Binary plot of As versus S in atoms per formula unit.

and the regression line is  $\text{Ni} = 0.744 - 0.792 \text{Co}$  ( $R = 0.91$ ).

The chemical composition of  $\text{GC}_{\text{ss}}$  I crystals (Table 5) ( $\text{Co}_{0.10-0.74}\text{Ni}_{0.07-0.80}\text{Fe}_{0.03-0.58})\text{As}_{0.95-1.20}\text{S}_{0.83-1.06}$ , shows an As:S ratio varying from 0.90 to 1.45 ( $1.07 \pm 0.11$ ), and a strong negative correlation between (Fe + Ni) and Co ( $R = -0.99$ ), indicative of their mutual substitution. Consequently,  $\text{GC}_{\text{ss}}$  I crystals display the same type of compositional trend as alloclasite, *i.e.*, a Ni/Fe trend characterized by the substitution of Co by a mixture of Ni and Fe (Fig. 5A), with the regression line  $\text{Ni} = 0.6013 - 0.56526 \text{Co}$  ( $R = 0.72$ ). The compositional fields of alloclasite and  $\text{GC}_{\text{ss}}$  I and the textural relationships (Fig. 2E) suggest that alloclasite was replaced by  $\text{GC}_{\text{ss}}$  I in a metal-rich environment (Hem *et al.* 2001) characterized by an increase in Fe and Ni concentration with a concomitant decrease in As concentration. Moreover, the overlap between the compositional fields of alloclasite and  $\text{GC}_{\text{ss}}$  I may be interpreted as a compositional continuum between alloclasite and the  $\text{GC}_{\text{ss}}$  I phase as Ni activity increased. The increase in Ni contents started with the crystallization of alloclasite instead of safflorite (Fig. 2E).

The phase  $\text{GC}_{\text{ss}}$  II ( $\text{Co}_{0.02-0.81}\text{Ni}_{0.10-0.96}\text{Fe}_{0.00-0.28})\text{As}_{1.01-1.36}\text{S}_{0.67-1.01}$  exhibits considerable compositional variability (Table 5) in the Fe-poor region of the system  $\text{CoAsS--NiAsS--FeAsS}$  (Fig. 6A). The As:S ratio ranges from 1.00 to 2.03 ( $1.43 \pm 0.31$ ). This variability is directly related to the Ni contents, as there is a posi-

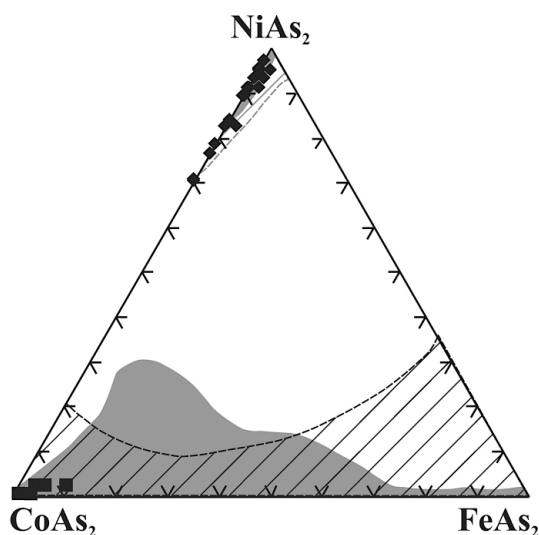


FIG. 4. Plot of diarsenide compositions in the system  $\text{CoAs}_2\text{--NiAs}_2\text{--FeAs}_2$ . Black squares: safflorite; black diamonds: rammelsbergite. The compositional limits of natural (Ni, Fe, Co) diarsenides according to Roseboom (1963) (dashed area) and Radcliffe & Berry (1968) (full area) are shown.

TABLE 4. STATISTICAL RESULTS OF ELECTRON-MICROPROBE ANALYSES OF ALLOCLASITE (STAGE III) AND COBALTITE (STAGE VI) FROM THE SAN JUAN DE PLAN DEPOSIT, CENTRAL PYRENEES, SPAIN

		Compositions (weight %)						Atoms per formula unit					
		S	As	Fe	Co	Ni	Total	S	As	Fe	Co	Ni	As#
Alo n = 81	min	16.37	45.02	0.32	17.99	0.00	98.53	0.88	0.99	0.02	0.52	0.00	0.50
	max	19.73	49.74	12.80	34.32	9.43	101.47	1.02	1.14	0.39	0.96	0.27	0.56
	mean	18.63	46.42	2.80	28.65	3.43	100.28	0.97	1.04	0.08	0.81	0.10	0.52
	36	17.91	46.47	6.39	24.80	3.65	100.09	0.95	1.05	0.19	0.71	0.10	0.53
	39	18.44	45.80	5.08	25.83	4.33	99.59	0.97	1.02	0.15	0.74	0.12	0.51
	66	18.21	46.16	1.92	30.49	2.70	99.77	0.96	1.04	0.05	0.87	0.08	0.52
	67	17.36	47.59	1.58	30.73	2.95	100.35	0.91	1.08	0.05	0.88	0.08	0.54
	68	18.65	45.96	4.48	27.99	2.76	101.01	0.97	1.02	0.13	0.79	0.08	0.51
	69	18.24	45.49	3.90	28.82	2.29	98.91	0.96	1.03	0.12	0.83	0.07	0.52
	71	18.58	45.30	12.80	17.99	3.66	98.60	0.98	1.01	0.39	0.52	0.10	0.51
	72	18.12	45.62	4.76	27.59	2.64	98.94	0.96	1.03	0.15	0.79	0.07	0.52
	73	17.40	46.93	5.90	25.98	2.70	99.60	0.92	1.07	0.19	0.75	0.08	0.54
	C103	18.55	46.65	1.86	27.67	4.87	99.75	0.98	1.04	0.05	0.79	0.13	0.51
	C108	18.85	46.56	1.42	26.98	6.01	99.99	0.98	1.03	0.05	0.77	0.17	0.51
	D21	19.22	46.46	1.88	26.66	5.54	99.12	0.97	1.06	0.05	0.77	0.15	0.52
D22	18.28	48.25	1.58	26.36	6.16	100.08	0.92	1.09	0.05	0.77	0.17	0.54	
D23	18.12	46.70	1.96	25.54	6.08	98.93	0.97	1.06	0.07	0.83	0.17	0.52	
D24	18.12	47.37	1.77	25.09	7.12	99.66	0.96	1.06	0.05	0.72	0.20	0.52	
D28	17.05	49.39	1.02	25.64	6.84	100.00	0.90	1.12	0.03	0.75	0.20	0.55	
D30	16.37	49.74	1.30	30.44	1.87	100.03	0.88	1.14	0.03	0.90	0.05	0.56	
Cbt n = 18	min	17.52	41.74	1.02	23.42	0.09	99.33	0.93	0.99	0.03	0.68	0.00	0.50
	max	19.70	48.13	4.19	33.10	9.26	101.34	1.01	1.08	0.13	0.93	0.27	0.54
	mean	18.96	45.88	2.38	29.94	2.57	100.60	0.99	1.02	0.07	0.85	0.08	0.51
	C153	19.15	45.94	2.66	32.02	0.45	100.56	0.99	1.01	0.08	0.90	0.02	0.51
	D56	19.29	46.50	2.25	32.42	0.09	100.66	0.99	1.03	0.07	0.91	0.00	0.51
	D59	19.22	45.82	1.29	33.10	0.41	100.07	1.00	1.02	0.03	0.93	0.02	0.50

Representative results of micro-analyses are indicated in Figures 2D, 2E, and 2F. As#: As/(As + S).

tive correlation between As and Ni ( $R = 0.70$ ). As a whole, the composition of GC<sub>ss</sub> II defines a chemical trend characterized by the substitution of Co by Ni which, according to Hem *et al.* (2001), is consistent with a significant increase in the As content. Phase GC<sub>ss</sub> II is overgrown by As-rich gersdorffite, and this was followed by the crystallization of rammelsbergite and skutterudite.

The arsenic-rich gersdorffite (Table 6) displays a narrow range in metal contents (Fig. 6A) and a broad variability in As and S contents:  $(\text{Ni}_{0.65-0.98}\text{Co}_{0.02-0.27}\text{Fe}_{0.00-0.06})\text{As}_{1.28-1.75}\text{S}_{0.28-0.77}$ . It shows a negative correlation between the sum Co + Fe and Ni content (Co/Fe trend) with a regression line  $\text{Ni} = 0.988 - 1.113(\text{Co} + \text{Fe})$ ,  $R = -0.93$ ). The assemblage in which this trend is found suggests an environment with a high fugacity of arsenic, as shown by Hem *et al.* (2001) in a magmatic deposit associated with the Ronda peridotite (Spain). There is no correlation among cations and anions, and the As:S ratio is very variable, suggesting that As content is independent of the metal content.

The textural relations among GC<sub>ss</sub> I, GC<sub>ss</sub> II and As-Gdf shown in Figure 2H, along with their compositions in the system NiAsS-CoAsS-FeAsS and the relation between As and Ni contents, have been plotted in Figures 6B and 6C. From GC<sub>ss</sub> I to As-Gdf, there is a significant increase in Ni and As contents. In Figures 6D and 6E (relating to Fig. 2G), the compositional varia-

tion between GC<sub>ss</sub> II and As-Gdf (Tables 5, 6) is shown. Both crystals display identical Ni contents, but As contents are much higher in As-Gdf. GC<sub>ss</sub> II and As-Gdf crystals show fine oscillatory growth-zoning characterized by small variations in As and S contents.

Cobaltite,  $(\text{Co}_{0.68-0.93}\text{Ni}_{0.00-0.27}\text{Fe}_{0.03-0.12})\text{As}_{0.99-1.08}\text{S}_{0.93-1.01}$ , displays a narrower compositional range than alloclasite (Table 4). Electron-microprobe analyses show a small excess of As over S, which is in disagreement with the findings of Maurel & Picot (1974). The amount of Co and the As:S ratio correlate negatively ( $R = -0.75$ ).

## DISCUSSION

### *Compositional trends and extent of solid solution in the system Ni-Co-Fe-As-S*

Mineralogical evidence suggests that the compositional trends exhibited by the Ni-Co-Fe phases found in the San Juan de Plan deposit, as well as the crystallization sequence, are linked to changes in activities of key elements in the mineralizing fluids. For example, the compositional variation in skutterudite shows that Ni and Fe substitute for Co in different proportions, depending on the paragenetic position of skutterudite (Fig. 3A). Skutterudite I, along with GC<sub>ss</sub> II (Fig. 6A), display a Ni-enrichment trend, marked by the replace-

ment of Co for Ni, which suggests high fugacities of the anion (As) (Hem *et al.* 2001). The sequential formation of GC<sub>ss</sub> II, As–Gdf, rammelsbergite and skutterudite II also show a crystallization trend characterized by the progressive increase in the As fugacity as a continuation of the Ni trend defined by GC<sub>ss</sub> II. In contrast, alloclasite, GC<sub>ss</sub> I and skutterudite II (Figs. 3A, 5A) display a Ni/Fe trend, in which Co is replaced by a mixture of Ni and Fe. The Ni/Fe trend indicates that these phases crystallized in a metal-rich environment (Hem *et al.* 2001).

If we take into account that alloclasite is paragenetically earlier than GC<sub>ss</sub> I, an increase in Ni activity during stage III should inhibit the precipitation of alloclasite, favoring instead the crystallization of GC<sub>ss</sub> I. This inference is in agreement with the idea that alloclasite forms under high As fugacity and moderate Ni activity (Maurel & Picot 1974). Where the activity of Ni increases, the deposition of alloclasite ceases,

which favors the precipitation of GC<sub>ss</sub> I. The overlap between the compositional fields of alloclasite and GC<sub>ss</sub> I, as well as their similar chemical trends, support this conclusion (Fig. 5A).

In comparison with available compositions of gersdorffite–cobaltite<sub>ss</sub> taken from the literature, our GC<sub>ss</sub> I data partly overlap those of Oen *et al.* (1971), Petruk *et al.* (1971), Gervilla & Rønsbo (1992) and Gervilla *et al.* (1998). On the other hand, the data of Wagner & Lorenz (2002) are similar to ours for GC<sub>ss</sub> II. Gersdorffite–cobaltite<sub>ss</sub> from the San Juan de Plan deposit shows variations in Ni:Fe ratio from 0 to 46.5, whereas the gersdorffite compositions of Wagner & Lorenz (2002) range between 0 and 44.0. These values indicate that both Fe and Ni are independent of each other, and that the constant Ni:Fe ratio is not an invariant feature of the ternary sulfarsenides (Hem 1998), which is in contrast with those trends reported in the literature: Béziat *et al.* (1996) determined an almost fixed

TABLE 5. STATISTICAL RESULTS OF ELECTRON-MICROPROBE ANALYSES OF GC<sub>ss</sub> I (STAGE III) AND GC<sub>ss</sub> II (STAGE IV) FROM THE SAN JUAN DE PLAN DEPOSIT, CENTRAL PYRENEES, SPAIN

		Compositions (weight %)						Atoms per formula unit					
		S	As	Fe	Co	Ni	Total	S	As	Fe	Co	Ni	As#
GC <sub>ss</sub> I n = 89	min	15.38	44.19	1.21	3.73	2.22	97.02	0.83	0.95	0.03	0.10	0.07	0.47
	max	21.13	51.93	20.03	25.78	27.20	101.75	1.06	1.20	0.58	0.74	0.80	0.59
	mean	18.71	46.59	8.26	11.75	14.50	100.09	0.97	1.04	0.25	0.33	0.41	0.52
	C10	20.50	45.30	12.20	9.27	13.40	100.75	1.04	0.97	0.36	0.26	0.37	0.48
	C12	20.20	44.95	11.70	6.55	17.00	100.64	1.03	0.98	0.34	0.18	0.47	0.49
	C13	20.30	45.43	11.60	8.07	15.60	100.64	1.02	0.98	0.34	0.23	0.44	0.49
	C16	21.10	44.19	12.60	5.84	16.80	100.94	1.06	0.95	0.37	0.16	0.47	0.47
	C104	19.40	46.31	7.29	21.30	6.78	101.12	0.98	1.02	0.21	0.59	0.20	0.51
	C105	16.20	49.48	1.21	16.00	13.40	99.53	1.01	1.10	0.03	0.46	0.39	0.52
	C119	20.50	48.00	5.65	16.10	12.70	100.21	1.05	0.98	0.16	0.44	0.36	0.48
	C120	20.10	45.36	12.80	9.73	12.70	100.89	1.02	0.98	0.37	0.27	0.35	0.49
	C122	18.70	47.26	7.31	10.10	16.40	99.78	0.97	1.06	0.22	0.28	0.47	0.52
	C180	20.00	44.58	12.70	6.44	15.50	99.63	1.02	0.99	0.38	0.18	0.43	0.49
	C181	20.40	44.55	12.70	7.48	14.20	99.54	1.05	0.97	0.38	0.21	0.39	0.48
	C185	20.00	45.25	12.40	8.01	14.50	100.23	1.02	0.98	0.36	0.23	0.41	0.49
	D25	18.20	47.86	3.19	20.10	10.90	100.53	0.95	1.07	0.10	0.57	0.32	0.53
	D26	18.10	46.91	3.43	23.00	7.57	99.41	0.96	1.06	0.10	0.66	0.22	0.52
D31	18.50	46.47	3.89	16.10	14.00	99.80	0.98	1.04	0.12	0.46	0.40	0.51	
GC <sub>ss</sub> II n = 119	min	11.84	45.39	0.01	0.58	3.45	98.10	0.67	1.01	0.00	0.02	0.10	0.50
	max	19.53	56.36	9.60	28.26	32.73	101.47	1.01	1.36	0.28	0.81	0.96	0.67
	mean	15.90	50.51	1.62	10.72	20.99	99.95	0.85	1.17	0.05	0.31	0.62	0.58
	B36	14.40	50.41	3.74	6.37	23.10	98.19	0.80	1.19	0.12	0.20	0.69	0.60
	C9	14.90	52.49	4.12	7.05	21.30	100.20	0.81	1.23	0.12	0.21	0.63	0.60
	C11	12.32	55.60	1.36	4.03	26.06	99.69	0.69	1.35	0.04	0.13	0.80	0.66
	C15	11.84	56.36	1.00	5.44	25.00	100.20	0.67	1.36	0.04	0.16	0.78	0.67
	C148	18.36	48.25	7.50	4.47	21.20	99.94	0.96	1.08	0.22	0.13	1.61	0.53
	C149	14.23	53.00	0.81	3.53	27.50	99.12	0.78	1.26	0.02	0.11	0.83	0.62
	C152	15.60	50.49	1.10	4.06	26.70	98.10	0.86	1.18	0.04	0.12	0.79	0.58
	C184	16.59	49.32	2.18	4.06	26.10	98.46	0.90	1.14	0.07	0.12	0.76	0.56
	D57	13.68	53.76	0.58	3.69	28.90	100.82	0.75	1.26	0.02	0.11	0.86	0.63
	D61	13.53	54.62	0.05	3.16	29.90	101.37	0.74	1.28	0.00	0.09	0.89	0.63
	D63	14.90	52.68	1.82	4.90	26.50	100.86	1.08	1.22	0.05	0.14	0.78	0.60
	D105	15.73	51.09	0.08	1.26	31.90	100.78	0.85	1.18	0.00	0.03	0.94	0.58
	D106	14.69	52.71	0.15	1.45	32.20	101.29	0.80	1.21	0.00	0.03	0.95	0.60
	D107	15.04	52.30	0.14	1.41	31.70	100.84	0.82	1.21	0.00	0.03	0.94	0.60
	D108	16.29	50.23	0.04	1.40	32.20	100.42	0.87	1.15	0.00	0.03	0.94	0.57
	D109	13.13	54.51	0.16	1.55	31.50	101.00	0.72	1.28	0.00	0.05	0.95	0.64
D110	14.85	52.98	0.02	1.48	31.23	100.56	0.80	1.23	0.00	0.05	0.93	0.61	
D169	13.87	53.62	0.05	6.76	26.41	100.73	0.75	1.26	0.00	0.19	0.79	0.63	

Representative results of micro-analyses have been indicated in Figures 2A, 2C, 2E, 2F, 2G, 2H, 2I, and 2J. As#: As/(As + S).

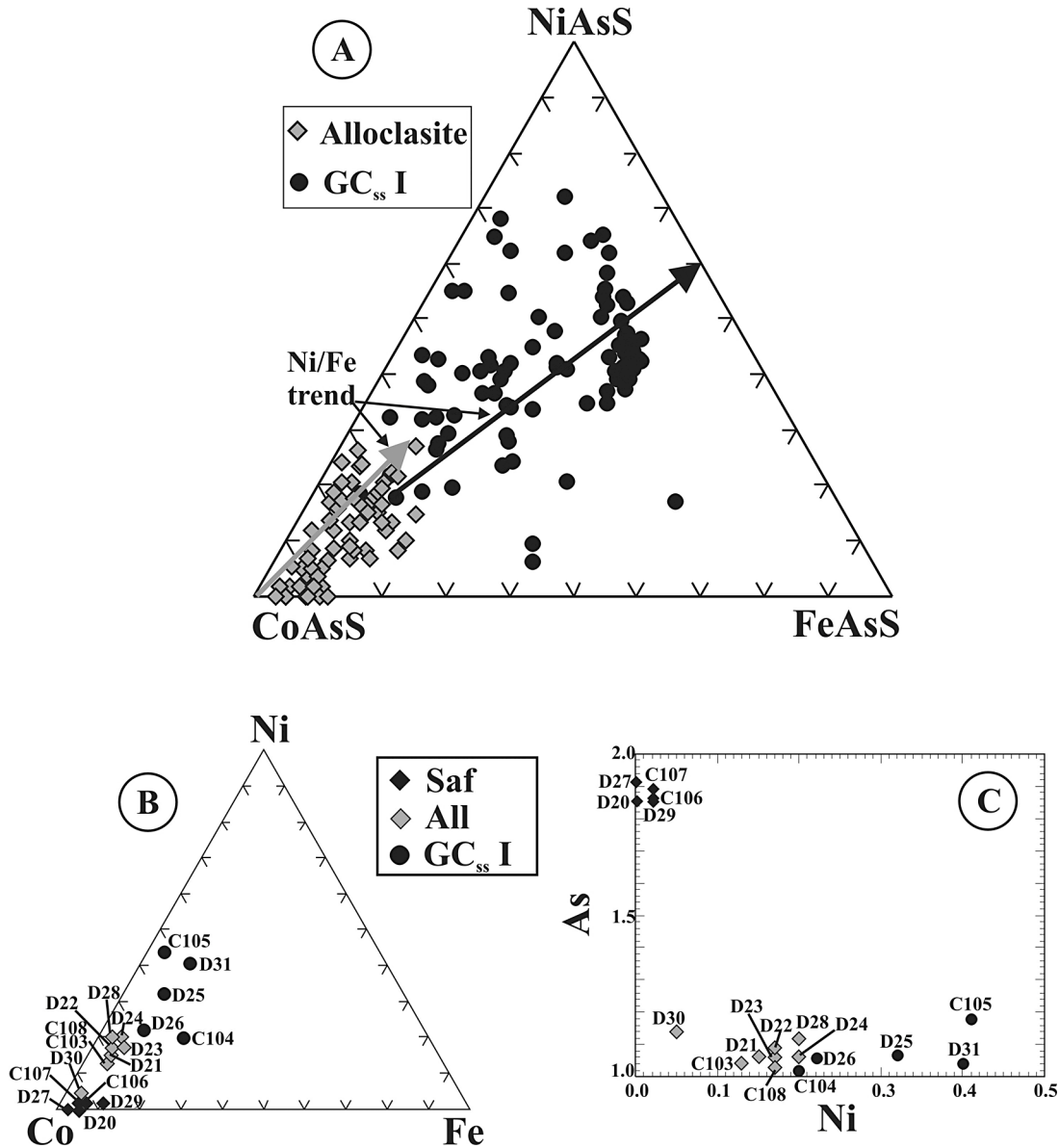


FIG. 5. A. Plot of the composition of alloclasite and GC<sub>ss</sub> I crystals in the system NiAsS–CoAsS–FeAsS (in atomic proportions). The arrows represent the trends that indicate the compositional variability in both minerals. B. Composition of safflorite, alloclasite and GC<sub>ss</sub> I in atomic proportions. The numbers represent the compositions listed in Tables 3, 4 and 5 and indicated in Figure 2E. C. Binary diagram showing the relationship between As and Ni in atoms per unit formula.

(Fe<sub>0.33</sub>Ni<sub>0.67</sub>) ↔ Co trend for solid solutions of cobaltite–gersdorffite with a Co content of 0.05 to 0.59, and corresponding trends are shown by the data of Mposkos (1983) and Gervilla *et al.* (1996). Fukuoka & Hirowatari (1980) found that the Fe<sub>0.35</sub>Ni<sub>0.65</sub> line defines the maximum Ni:Fe ratio. Béziat *et al.* (1996) argued that it was

caused by the substitution of 3 Co atoms by 2 Ni atoms and 1 Fe atom.

With regard to As:S ratio, the San Juan de Plan gersdorffite–cobaltite<sub>ss</sub> shows narrower ranges (GC<sub>ss</sub> I: 0.9 to 1.45, GC<sub>ss</sub> II: 1.00 to 2.03) than those values (0.78 to 2.44) reported previously by Barkov *et al.* (1999, and

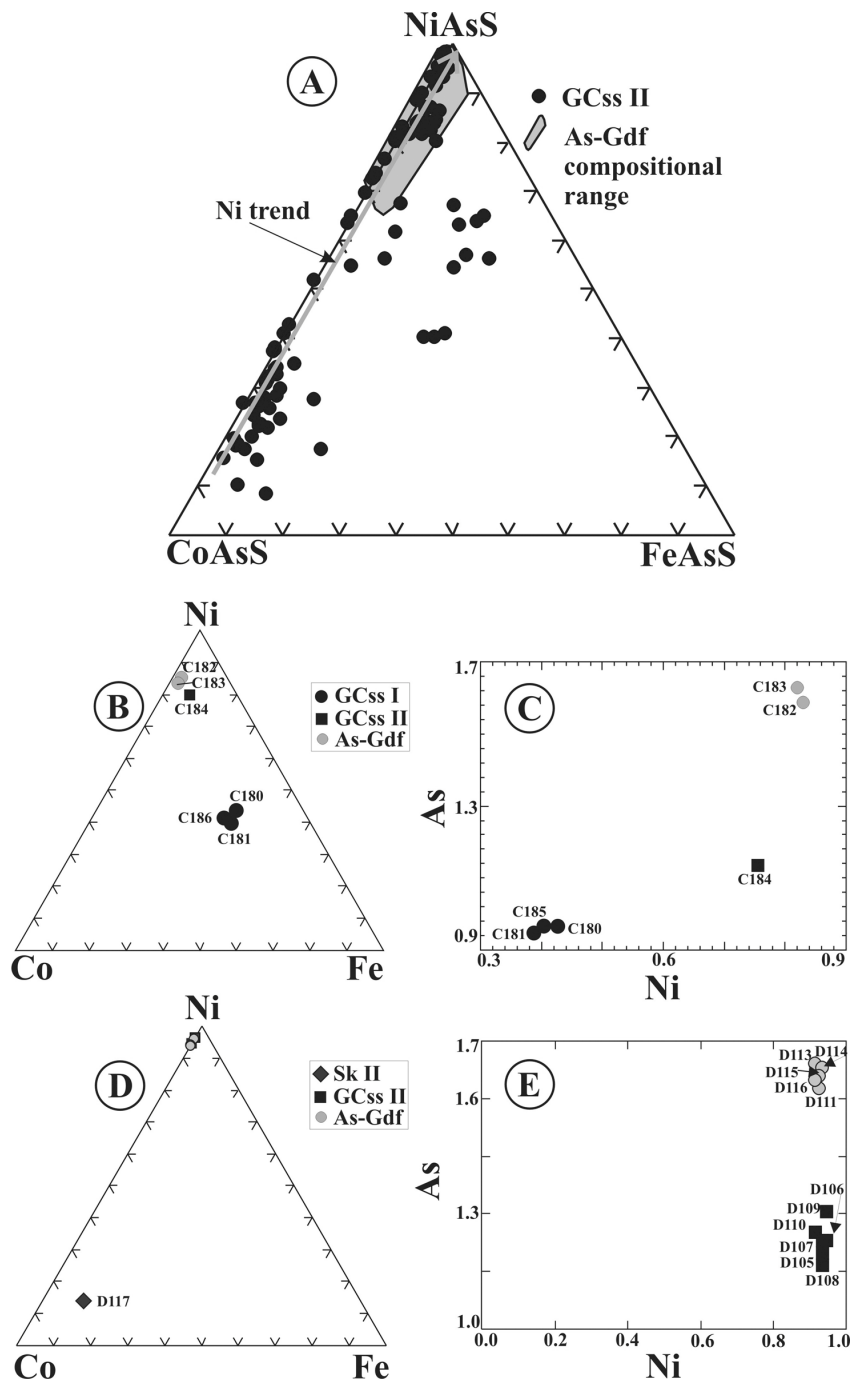


FIG. 6. A. Composition of GC<sub>ss</sub> II and As-Gdf crystals in the system NiAsS-CoAsS-FeAsS. The arrow represents the Ni trend. B. Composition of GC<sub>ss</sub> I, GC<sub>ss</sub> II and As-Gdf in atomic proportions. The numbers refer to compositions listed in Tables 5 and 6 and indicated in Figure 2H. C. Binary diagram showing the relationship between As and Ni in atomic proportions. D. Composition of GC<sub>ss</sub> II, As-Gdf and Sk II (atomic proportions) for the case of figure 2G. E. Binary diagram showing the compositional variation in As and Ni contents (in atoms per unit formula) between GC<sub>ss</sub> II and As-Gdf crystals, from Figure 2G.

TABLE 6. STATISTICAL RESULTS OF ELECTRON-MICROPROBE ANALYSES OF ARSENIC-RICH GERSDORFFITE (As-Gdf, STAGE IV) FROM THE SAN JUAN DE PLAN DEPOSIT, CENTRAL PYRENEES, SPAIN

	Compositions (weight %)						Atoms per formula unit						
	S	As	Fe	Co	Ni	Total	S	As	Fe	Co	Ni	As#	
As-Gdf	min	4.43	53.44	0.00	0.53	20.08	98.12	0.28	1.28	0.00	0.02	0.65	0.62
<i>n</i> = 157	max	13.85	66.29	1.66	8.61	30.88	101.38	0.77	1.75	0.06	0.27	0.98	0.89
	mean	8.33	60.81	0.27	3.21	26.76	99.74	0.49	1.54	0.01	0.10	0.86	0.78
B40		6.53	62.63	0.32	2.43	27.14	99.31	0.39	1.63	0.02	0.08	0.89	0.81
C121		11.92	56.04	0.84	6.92	22.83	98.70	0.67	1.36	0.04	0.22	0.71	0.67
C150		5.78	64.54	0.06	2.60	25.58	98.65	0.36	1.70	0.00	0.08	0.87	0.83
C151		7.05	62.43	0.08	2.48	26.20	98.56	0.43	1.62	0.00	0.08	0.88	0.79
C154		5.24	64.93	0.00	2.20	26.01	98.4	0.32	1.73	0.00	0.08	0.87	0.84
C182		7.50	61.94	0.47	3.26	25.06	98.41	0.44	1.60	0.00	0.12	0.83	0.78
C183		6.52	63.24	0.47	3.85	24.67	99.07	0.39	1.64	0.00	0.14	0.82	0.81
D58		6.03	64.58	0.07	2.51	27.76	101.05	0.37	1.65	0.00	0.08	0.90	0.82
D60		5.97	64.43	0.05	2.68	28.04	101.20	0.36	1.63	0.00	0.09	0.91	0.82
D62		5.74	65.17	0.03	2.48	27.78	101.38	0.35	1.67	0.00	0.08	0.90	0.83
D111		7.46	62.49	0.00	1.80	28.79	100.68	0.44	1.58	0.00	0.06	0.93	0.78
D113		6.26	64.08	0.08	1.56	28.37	100.52	0.38	1.64	0.00	0.06	0.92	0.81
D114		6.46	63.53	0.05	1.44	28.73	100.27	0.38	1.63	0.00	0.04	0.94	0.81
D115		6.64	63.73	0.06	1.49	28.73	100.90	0.40	1.61	0.00	0.06	0.93	0.80
D116		7.17	62.54	0.13	0.56	28.29	99.89	0.42	1.60	0.00	0.06	0.92	0.79
D170		6.37	63.59	0.04	1.89	28.63	100.42	0.38	1.62	0.00	0.06	0.94	0.81
D171		7.52	62.25	0.08	1.83	28.91	100.84	0.44	1.58	0.00	0.06	0.93	0.78

Representative results of micro-analyses are indicated in Figures 2C, 2F, 2G, 2H, and 2J. As#: As/(As + S).

references therein) and Béziat *et al.* (1996, and references therein). However, the As:S ratio of GC<sub>ss</sub> II is similar to that of Wagner & Lorenz (2002), which varies from 1.23 to 1.76. The experimental results of Maurel & Picot (1974), and the data reported by Béziat *et al.* (1996) and Barkov *et al.* (1999), show that the degree of substitution of As for S increases with increasing (Ni + Fe) content, which contrasts with our results.

In order to know the scheme of substitution in the GC<sub>ss</sub> crystals, the limits of substitution, and the compositional trends related to such substitutions, we have plotted *Me* (Ni or Co contents *versus* As<sub>total</sub> - As<sub>MeAsS</sub> (Figs. 7A, B). Thus, the covariation between *Me* and As contents, as well as the deviation from [AsS]<sup>3-</sup> toward either [As<sub>2</sub>]<sup>4-</sup> or [S<sub>2</sub>]<sup>2-</sup> anionic pairs, is revealed. Thin dotted lines in Figures 7A and 7B represent *MeAs*<sub>2</sub>, *MeAsS* and *MeS*<sub>2</sub> binary systems in which anionic content is stoichiometric, *i.e.*, only cationic substitution is allowed. Thick dashed and solid lines show regression lines for GC<sub>ss</sub> I and GC<sub>ss</sub> II, respectively. Since regression lines are not parallel to stoichiometric lines, cations and anions are mutually dependent and, therefore, a coupled substitution (*MeAsS* ↔ *MeAs*<sub>2</sub> or *MeAsS* ↔ *MeS*<sub>2</sub>) is deduced. The slope of regression lines provides information about the proportion of each pattern of substitution; thus, in Figure 7A, the value 1.25929 for GC<sub>ss</sub> II indicates that the contribution of coupled substitution [(Co,Fe)AsS ↔ NiAs<sub>2</sub>] is *ca.* 25% of the total. In the case of GC<sub>ss</sub> I, the contribution of the coupled substitution is smaller. In Figure 7B, the ordinate gives the As content related to Co content after considering the As contribution linked to Ni content (see Fig. 7A), and to stoichiometric FeAsS. The relationship between regres-

sion and stoichiometric lines in GC<sub>ss</sub> I crystals indicates that the Co-free end-member has an As deficit of *ca.* 0.1 *apfu*, *i.e.*, there is CoAsS ↔ FeS<sub>2</sub> substitution. However, from the crossover point between the above lines (0.6 Co *apfu*) upward, there exists a surplus of As. In addition, the slope of 1.17003 for the Co-end member indicates that the extent of substitution CoAsS ↔ CoAs<sub>2</sub> is *ca.* 7%. Consequently, it could be deduced that the increase in [S<sub>2</sub>]<sup>2-</sup> is linked to the introduction of Fe into the GC<sub>ss</sub> I structure. With regard to the GC<sub>ss</sub> II data, the slope (1.0262) of the regression line that runs parallel to the CoAsS stoichiometric line indicates that cationic substitution is the only scheme of substitution.

To sum up, the scheme of substitution of GC<sub>ss</sub> I and GC<sub>ss</sub> II crystals is slightly different; it indicates a positive correlation between S and Fe contents, and Co and As contents, in GC<sub>ss</sub> I crystals, whereas GC<sub>ss</sub> II crystals show a positive correlation between As and Ni contents. From Figures 7A and 7B, it follows that GC<sub>ss</sub> II is more As-rich than GC<sub>ss</sub> I, and that the highest As:S ratio corresponds to Fe-free GC<sub>ss</sub> II. Consequently, following Hem *et al.* (2001), we believe that these variations are related to the As fugacity in the mineralizing fluids. An increase in the As fugacity during deposition of GC<sub>ss</sub> II favored the incorporation of Ni in GC<sub>ss</sub> II instead of Co (Ni trend). Thus, a higher fugacity of As in the fluid results in a higher content of As and Ni in the crystallizing mineral. This enrichment resulted in the subsequent crystallization of As-rich gersdorffite and ramelsbergite during stage IV.

Another discrepancy among our data and the experimental data reported in literature concerns the compositional variability of sulfarsenides and diarsenides. Yund

(1962) determined that the gersdorffite solid-solution extends along a line from rammelsbergite ( $\text{NiAs}_2$ ) to vaesite ( $\text{NiS}_2$ ) in the system Ni–As–S. Likewise, Yund (1962) determined experimentally that the maximum As content of gersdorffite corresponds to the formula  $\text{NiAs}_{1.77}\text{S}_{0.23}$  (66.74 wt% As and 3.71 wt% S), whereas the maximum S content of rammelsbergite is  $1.1 \pm 0.1$  wt% at  $700^\circ\text{C}$  ( $\text{As}_{1.93}\text{S}_{0.07}$ ). Consequently, Yund (1962) proposed a miscibility gap between  $\text{As}_{1.93}\text{S}_{0.07}$  and  $\text{As}_{1.77}\text{S}_{0.23}$ . However, Spiridonov & Chvileva (1995) found a complete solid-solution between gersdorffite and krutovite (cubic  $\text{NiAs}_2$ ) in samples from the Manybay U–Mo deposit, in Kazakhstan. Recently, Hem & Makovicky (2004) found experimentally a nickel diarsenide containing 12–14 at.% S marked by optical similarity with gersdorffite, which confirmed the existence of krutovite (cubic  $\text{NiAs}_2$  phase, *Pa3*). Electron-microprobe analyses (Figs. 7C, D) seemingly show that

there exists a compositional continuum between rammelsbergite and gersdorffite. However, microscopic observations (complex twinning) suggest to us that rammelsbergite is a product of inversion of krutovite. Consequently, our study supports the findings of Spiridonov & Chvileva (1995) on the complete solid-solution between gersdorffite and krutovite.

With regard to the compositional variability of gersdorffite, Choi & Imai (1985) reported an arsenic content of 63 wt% ( $\text{As}_{1.61}\text{S}_{0.37}$ ). Arsenic contents of gersdorffite in the literature are invariably lower than those of gersdorffite from San Juan de Plan (66.29 wt%), which, in turn, is as high as that experimentally proposed by Yund (1962). Consequently, the As:S ratio in our gersdorffite spans a range from 2.14 to 6.25, which is broader than that found in the literature [Bayliss (1982): 0.97 to 2.44, Petruk *et al.* (1971): 1.15 to 4.0, Choi & Imai (1985): 1.02 to 4.35, Vinogradova *et al.* (1974):

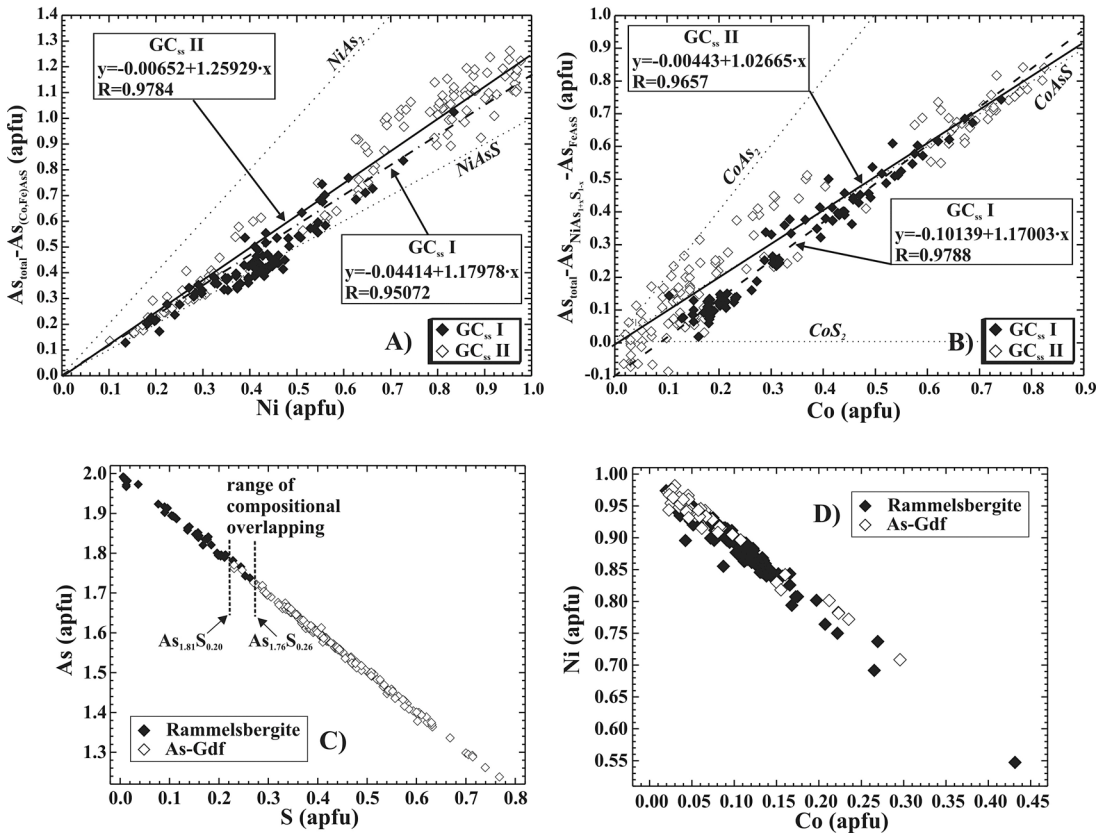


FIG. 7. A. Plot of  $\text{As}_{\text{total}} - \text{As}_{(\text{Co,Fe})\text{AsS}}$  versus Ni, in atoms per formula unit, for GC<sub>ss</sub> crystals. Regression lines with their R values along with the *MeAs*<sub>2</sub>, *MeAsS* and *MeS*<sub>2</sub> binary systems have also been represented. B. Plot of  $\text{As}_{\text{total}} - \text{As}_{\text{NiAs}_{1+x}\text{S}_{1-x}} - \text{As}_{\text{FeAsS}}$  versus Co, in atoms per formula unit. C. Plot of As versus S (in atoms per formula unit) for rammelsbergite (solid diamond) and arsenic-rich gersdorffite (open diamond). D. Binary diagram showing the relationship between Ni and Co in atoms per formula unit for the aforementioned minerals.

1.5 to 2.4, Wagner & Lorenz (2002): 1.26 to 1.77, Oen *et al.* (1971), Ixer *et al.* (1979), Permingeat & Zehni (1988), Gervilla & Rønsbo (1992), Béziat *et al.* (1996), Barkov *et al.* (1999): <1.44]. Figure 8 shows that sulfarsenides have low Ni contents, whereas the value As:S is close to 1. However, as this ratio increases, so does the Ni content, displaying a continuous variation of the As:S ratio from GC<sub>ss</sub> II to As-rich gersdorffite and rammelsbergite. Data in Figure 8 also suggest that As–Gdf represents the As-rich limit of GC<sub>ss</sub> II at 650°C, according to the experimental results of Hem & Makovicky (2004). These results further support the conclusion that both As and Ni contents in gersdorffite–cobaltite<sub>ss</sub> are controlled by the As fugacity of the mineralizing fluid at high temperature.

Figure 9 shows the binary presentation of the sides of the  $MX_2$  prism at 650°C from Hem & Makovicky (2004), with the solid lines showing the limits in solid solution for a given association of phases. The compositions of rammelsbergite, As–Gdf, GC<sub>ss</sub> I and GC<sub>ss</sub> II from San Juan de Plan deposit have been plotted in this diagram. GC<sub>ss</sub> I and GC<sub>ss</sub> II display a solid solution that fills the gersdorffite–cobaltite field obtained by Hem & Makovicky (2004), though, as we have noted, the As contents are higher than in our samples. In addition, As–Gdf and rammelsbergite compositions not only overlap

the solid-solution field between gersdorffite and krutovite–rammelsbergite, but also extend toward compositions richer in As and Co plus Fe than those investigated by Hem & Makovicky (2004). This fact also supports the hypothesis that the presence of rammelsbergite instead of krutovite in San Juan de Plan ores may be due to the inversion of krutovite to rammelsbergite.

In the San Juan de Plan ores, the assemblage crystallized during stage IV resembles that described by Hem & Makovicky (2004) at 650°C (Fig. 9), since small-scale bands of As-rich gersdorffite containing up to 51.94 at.% As alternate in zoned crystals with another Ni diarsenide (Fig. 2G). This finding may explain the larger extension of our As–Gdf data toward the compositions rich in As for the homogeneous phases plotted in Figure 2G.

#### Conditions of ore formation

The paragenetic sequence at San Juan de Plan is shown with the variation in arsenic fugacity during the precipitation of the different paragenetic stages in Figure 1. Keeping in mind that the arsenopyrite studied fulfills the criteria of Kretschmar & Scott (1976) and Sharp *et al.* (1985), that the minor element content is

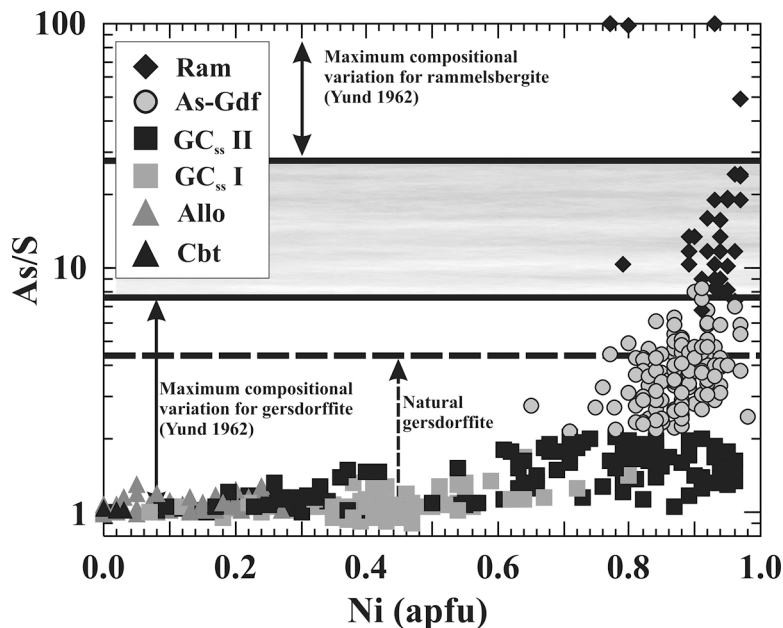


FIG. 8. As/S relationship versus Ni (in atoms per unit formula) in a linear-log scale. Solid lines represent empirical compositional limits for rammelsbergite and gersdorffite (Yund 1962). The dashed line shows the maximum compositional variation in gersdorffite found in the literature. The shaded area represents the hypothetical miscibility-gap between rammelsbergite and gersdorffite.

less than 1 wt% and there is no textural zoning, the extent of As-for-S substitution has been used as a geothermometer. It yields a range of temperatures of formation between 325 and 425°C for stage I. At this temperature,  $\log f(S_2)$  ranges between  $-9.2$  and  $-6.2$  for the given phase-assemblage.

The crystallization of nickeline, skutterudite I and safflorite during stage II provide strong support for a decrease in  $f(S_2)$  and, therefore, a strong increase in  $f(As)$ . According to Hem & Makovicky (2004), Co-rich safflorite at 650°C exhibits a maximum sulfur content of 0.18 apfu (5.92 at.%), whereas at 500°C it can contain up to 5.1 at.% S. The maximum sulfur content of safflorite from San Juan de Plan, 0.16 apfu (5.37 at.%), suggests formation temperatures close to 550°C.

According to the experiments of Maurel & Picot (1974) and Hem & Makovicky (2004), the maximum temperature of ore formation should have been reached when alloclasite was deposited during stage III and in stage IV during the crystallization of As-rich gersdorffite coexisting with rammelsbergite. The reported temperatures of alloclasite crystallization vary from 300–400°C (Ixer *et al.* 1979) to 450–600°C (Petruk *et al.* 1971). Nevertheless, Maurel & Picot (1974) found alloclasite to be a high-temperature phase, coexisting with cobaltite or safflorite at temperatures above 800°C. They also found that alloclasite is stable only on the As-rich side of the  $CoS_2$ – $CoAs_2$  binary join and, consequently, an excess of As is necessary for the formation of this mineral; on the other hand, high Ni contents inhibit the formation of alloclasite owing to the neutralization of As by Ni where the ratio 1:1 between them is reached. Our data partially agree with the results of Maurel & Picot (1974), since alloclasite in the

San Juan de Plan deposit are enriched in As and displays low Ni contents. Hem & Makovicky (2004) found that the As content of alloclasite, at 650°C, varies from 37 to 54 at.%, and between 42 and 52 at.% at 500°C (our compositions range between 33 and 38 at.%). However, Hem & Makovicky (2004) recognized that their alloclasite is more enriched in As than that found in nature. The high As content of the alloclasite analyzed by Hem & Makovicky (2004) with respect to that in the San Juan de Plan ores could indicate that the latter represent a S-rich extension of the alloclasite solid-solution field. Regarding Fe, Co, and Ni, Hem & Makovicky (2004) found that at 650°C, Co is completely replaced by a mixture of Fe and Ni, whereas at 500°C, both elements show a limited solubility (Fe < 1.4 at.%, Ni < 2.8 at.%). In our samples, Fe is less than 13.0 at.% and Ni, less than 8.8 at.%, which equates to a temperature formation of alloclasite at San Juan de Plan between 650° and 550°C. This estimate must be treated with caution because, as noted above, alloclasite from San Juan de Plan ores crystallized in an environment richer in S than that studied by Hem & Makovicky (2004). However, the value of the  $c$  parameter of graphite (between 6.7157 and 6.7211 Å) from stylolitic graphite seams linked to the ore horizon has been used as a geothermometer (Shengelia *et al.* 1977). Calculated temperatures range between 650° and 550°C.

The compositions of  $GC_{ss}$  I plot within the 650°C immiscibility region (Fig. 10A) in the system NiAsS–CoAsS–FeAsS (Klemm 1965b). Misra & Fleet (1975), Oen *et al.* (1984), and Hem *et al.* (2001) obtained contradictory temperatures when they applied Klemm's geothermometer. Misra & Fleet (1975) suggested that Klemm (1965b) did not take into account the As-for-S

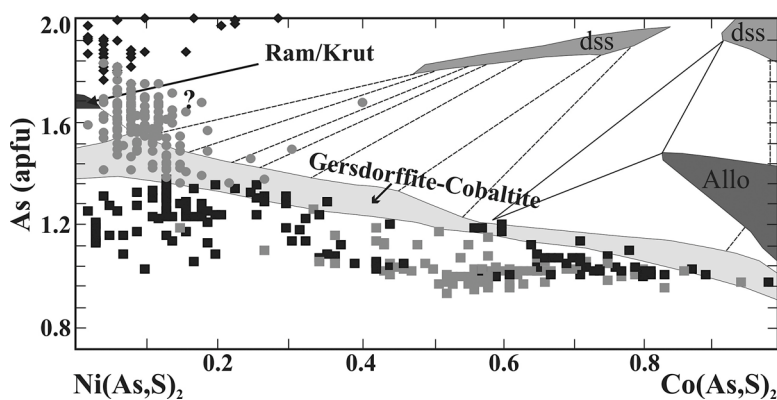


FIG. 9. The concentration of As (atoms per formula unit) versus compositional variations in terms of Ni-(Co+Fe) for rammelsbergite (black diamond), As–Gdf (grey circle),  $GC_{ss}$  I (grey square) and  $GC_{ss}$  II (black square). Diarsenides formed at 650°C in equilibrium with sulfarsenides and their solid-solution fields from Hem & Makovicky (2004) have also been represented.

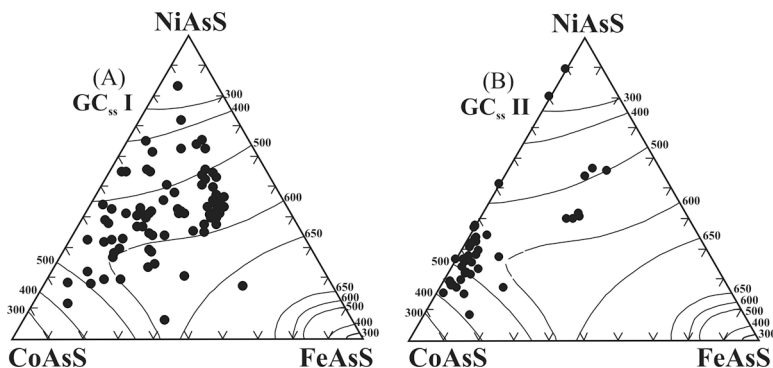


FIG. 10. Compositional plot of GC<sub>ss</sub> I (A) and GC<sub>ss</sub> II (B) in the system NiAsS–CoAsS–FeAsS. Solvus lines at different temperatures are taken from Klemm (1965b).

substitution, which adds a degree of variance to the system, making his solvus diagram useless for geothermometry. Hem & Makovicky (2004) found a nearly complete solid-solution between gersdorffite and cobaltite, again at 650°C, with a linear correlation between As and Ni and a negative correlation between Fe and As. At 500°C, the solid solution is very limited, and gersdorffite can contain up to 2.8 at.% Fe and 5.4 at.% Co, whereas the As content is very high with respect to natural samples. As can be seen in Figure 5A, the GC<sub>ss</sub> I compositions show intermediate compositions between gersdorffite and cobaltite end-members, having Fe and Ni contents up to 19 and 26 at.%, respectively, and with a negative correlation between As and Fe. These data suggest that GC<sub>ss</sub> I formed after alloclastite under similar conditions of temperature.

During the formation of the stage-IV ore assemblage (GC<sub>ss</sub> II, As–Gdf and rammelsbergite), the activity of arsenic increased without variations in the temperature. Although the rammelsbergite–pararammelsbergite inversion occurs at 590°C for pure NiAs<sub>2</sub>, the substitution of approximately 1 wt% S for As lowers the inversion temperature to 475 ± 25°C (Yund 1962). As both Co and Fe also probably lower the inversion temperature, taking into account the compositions of San Juan de Plan rammelsbergite, the temperature of crystallization in the present assemblage must have remained close to 500–600°C. When Klemm (1965b) investigated the temperature dependence of the (Fe,Co,Ni)AsS solid-solutions and suggested their application as a geothermometer, he did not deal with the As-for-S substitution. Consequently, if we try to apply his results, we must first leave out all those GC<sub>ss</sub>II compositions with As/S greater than 1. Thus, the compositional GC<sub>ss</sub> II data plotted in NiAsS–CoAsS–FeAsS space are located within the 600°C immiscibility region (Fig. 10B).

During stage V, the activity of arsenic in the mineralizing fluids was as high as in stage IV, with the for-

mation of skutterudite II. Both mineralogy and petrography from stage VI support a low-temperature deposition. The assemblage bismuthinite – native bismuth – pyrite indicates temperatures close to 271°C (melting point of native bismuth), with log  $f(S_2)$  of ca. –10.

In spite of a temperature of formation of approximately 600°C for the San Juan de Plan deposit deduced from phase relations (Yund 1962, Klemm 1965b, Hem & Makovicky 2004), the field data do not support such a high temperature. Subsequent geochemical studies on black shales, along with infrared microthermometry studies currently underway, should be able to test whether the deduced evolution of temperature in this study represent “true” conditions of deposition or a later process of re-equilibrium at low temperatures.

Jochum (2000) showed that the precipitation of sulfides minerals in vein systems is probably related to thermochemical processes of sulfate reduction during interaction of the hydrothermal fluids with organic matter in the wallrock. The distinctive spatial association of the Co–Ni–Fe enrichments in the San Juan de Plan ore with the Silurian black shales suggests a genetic link between the style of mineralization and this particular host-rock. The abundant organic matter in the black shales could have acted as a reducing agent for dissolved oxidized sulfur and arsenic species in the hydrothermal fluids, which would have resulted in the deposition of Co–Ni–Fe triarsenides, diarsenides, arsenides and sulfarsenides in close proximity to the contact between the ankerite-rich horizon and the top of Silurian black shales.

#### CONCLUSIONS

The present study reveals the existence of some discrepancies between our results and those reported in the literature for the system Co–Ni–Fe–As–S. These discrepancies pertain to the following themes.

a) The limited miscibility between gersdorffite and rammelsbergite. Electron-microprobe analyses seem to show that there exists a compositional continuum between rammelsbergite and gersdorffite. However, according to our microscope observations, the presence of rammelsbergite in San Juan de Plan ores may be due to the inversion of krutovite after rammelsbergite. Consequently, our findings support those of Spiridonov & Chvileva (1995) on the complete solid-solution between gersdorffite and krutovite.

b) An almost fixed ( $\text{Fe}_{0.33}\text{Ni}_{0.67}$ ) ↔ Co trend for solid solutions of cobaltite–gersdorffite. Gersdorffite–cobaltite<sub>ss</sub> from the San Juan de Plan deposit shows the largest variations in Ni:Fe ratio found in the literature, which indicates that Fe and Ni are independent of each other. Therefore, the constant Ni:Fe ratio is not a necessary feature of the ternary sulfarsenides studied.

c) The degree of substitution of As for S increases with increasing (Ni + Fe) content. The correlation between  $\text{As}_{\text{total}} - \text{As}_{\text{MeAsS}}$  and *Me* reveals the scheme of substitution and, therefore, the compositional trends related to such substitutions. The coupled substitution  $(\text{Co,Fe})\text{AsS} \leftrightarrow \text{NiAs}_2$  in  $\text{GC}_{\text{ss}}$  II crystals represents ca. 25% of the total [*i.e.*,  $(\text{Co,Fe})\text{AsS} \leftrightarrow \text{NiAsS}$  represents ca. 75%]. However, in  $\text{GC}_{\text{ss}}$  I crystals, the substitution  $\text{CoAsS} \leftrightarrow \text{FeS}_2$  is ca. 10%, whereas the substitution  $\text{CoAsS} \leftrightarrow \text{CoAs}_2$  is ca. 7%. In short, in  $\text{GC}_{\text{ss}}$  I crystals, there is a positive correlation between S and Fe contents, and Co and As contents, whereas  $\text{GC}_{\text{ss}}$  II crystals show a positive correlation between As and Ni contents.

d) Natural samples of skutterudite can have a small but real deficiency in As. A representative number of skutterudite samples analyzed from San Juan de Plan do not show such a deficiency.

The formation of the San Juan de Plan deposit can be divided into six stages, as summarized here. *Stage I*: pyrite I and arsenopyrite precipitate at temperatures between 325° and 425°C, with  $\log f(\text{S}_2)$  ranging between –9.2 and –6.2. *Stage II*: nickeline, skutterudite I and safflorite were formed, which corresponded to a drop in  $f(\text{S}_2)$ . The maximum sulfur content of safflorite from San Juan de Plan may indicate that it formed at temperatures close to 500°C. *Stage III*: the crystallization of allosclerite and  $\text{GC}_{\text{ss}}$  I crystals was characterized by a metal-rich environment and a high activity of anions, with temperatures close to 600°C. *Stage IV*:  $\text{GC}_{\text{ss}}$  II crystals, As–Gdf, and rammelsbergite are formed at constant temperatures, whereas the Ni and anion activities increased. *Stage V* represents an increase in the activity of As with the precipitation of skutterudite II. *Stage VI* began with the formation of cobaltite and bismuthinite, which led to the subsequent precipitation of pyrite II, chalcopyrite, and native bismuth at temperatures below 271°C, and the  $\log f(\text{S}_2)$  was ca. –10.

The source of the mineralizing fluid is enigmatic; it could be a residual magmatic fluid migrating through the pile of sedimentary rocks, but further conclusions on the exact nature and genesis of this fluid should be

deferred. The abundant organic matter in the black shales of the wallrock could have acted as a reducing agent for dissolved oxidized sulfur and arsenic species in the ore-bearing fluids, which would have resulted in the deposition of Co–Ni–Fe triarsenides, diarsenides, arsenides and sulfarsenides in close proximity to the contact between the ankerite-rich horizon and the top of Silurian black shales.

#### ACKNOWLEDGEMENTS

The authors are indebted to E. Makovicky for critical comments and corrections that greatly improved the manuscript. The reviewers, R.A. Ixer, S.R. Hem, R.F. Martin and P.G. Spry, are especially acknowledged for their constructive comments, which greatly contributed to the improvement of the original manuscript. This project was financially supported by Gobierno de Aragón (P2000/013). We thank the Asociación Mineralógica Aragonesa for access to material of private collections. Preliminary studies from San Juan de Plan deposit were undertaken by I.F. and I.S. as a part of a research project at Universidad de Zaragoza (221–139).

#### REFERENCES

- BARKOV, A.Y., THIBAUT, Y., LAAJOKI, K.V.O., MELEZHNIK, V.A. & NILSSON, L.P. (1999): Zoning and substitutions in Co–Ni–(Fe)–PGE sulfarsenides from the Mount General' skaya layered intrusion, Arctic Russia. *Can. Mineral.* **37**, 127–142.
- BAYLISS, P. (1982): A further crystal structure refinement of gersdorffite. *Am. Mineral.* **67**, 1058–1064.
- BÉZIAT, D., MONCHOUX, P. & TOLLON, F. (1996): Cobaltite–gersdorffite solid solution as a primary magmatic phase in spessartite, Lacaune area, Montagne Noire, France. *Can. Mineral.* **34**, 503–512.
- CASTROVIEJO, R. & NODAL, T. (1985): Estudio geológico de las concentraciones de Co–(Ni–Cu–Fe) en el Silúrico de San Juan de Plan, valle de Gistaín (Pirineo Huesca). *Bol. Geol. Min.* **46**, 607–625.
- CHOI, SEON-GYN & IMAI, N. (1985): Ni–Fe–Co arsenides and sulfarsenides from the Ulsan mine, Republic of Korea. *Mining Geol.* **35**, 1–16.
- FUKUOKA, M. & HIROWATARI, F. (1980): On minerals in the system Ni–Co–As–S from the bedded manganese ore deposits in the eastern part of Yamaguchi Prefecture; on the chemical compositions of gersdorffite–cobaltite solid solution. *Sci. Rep. Fac. Sci., Kyushu Univ., Geology* **13**, 239–249.
- GERVILLA, F., LEBLANC, M., TORRES-RUIZ, J. & FENOLL HACH-ALÍ, P. (1996): Immiscibility between arsenite and sulfide melts: a mechanism for concentration of noble metals. *Can. Mineral.* **34**, 485–502.

- \_\_\_\_\_, PAPUNEN, H., KOJONEN, K. & JOHANSON, B. (1998) Platinum-palladium- and gold-rich arsenide ores from the Kylmäkoski Ni-Cu deposits (Vammala Nickel Belt, SW Finland). *Mineral. Petrol.* **64**, 163-185.
- \_\_\_\_\_, & RØNSBO, J. (1992): New data on (Ni,Fe,Co) diarsenides and sulfarsenides in chromite-nicolite ores from Malaga Province, Spain. *Neues Jahrb. Mineral., Monatsh.*, 193-206.
- HEM, S.R. (1998): *The Ore Mineralogy of the Arroyo de la Cueva Deposits, Ronda Massif, Southeast Spain*. Cand. Scient. thesis, Univ. of Copenhagen, Copenhagen, Denmark.
- \_\_\_\_\_, & MAKOVICKY, E. (2004): The system Fe-Co-Ni-As-S. II. Phase relations in the (Fe,Co,Ni)As<sub>1.5</sub>S<sub>0.5</sub> section at 650° and 500°C. *Can. Mineral.* **42**, 63-86.
- \_\_\_\_\_, \_\_\_\_\_ & GERVILLA, F. (2001): Compositional trends in Fe, Co and Ni sulfarsenides and their crystal-chemical implications; results from the Arroyo de la Cueva deposits, Ronda Peridotite, southern Spain. *Can. Mineral.* **39**, 831-853.
- IXER, R.A., STANLEY, C.J. & VAUGHAN, D.J. (1979): Cobalt-, nickel-, and iron-bearing sulfarsenides from the north of England. *Mineral. Mag.* **43**, 389-395.
- JOCHUM, J. (2000): Variscan and post-Variscan lead-zinc mineralization, Rhenish Massif, Germany: evidence for sulphide precipitation via thermochemical sulphate reduction. *Mineral. Deposita* **35**, 451-464.
- KLEMM, D.D. (1965a): Untersuchung mit der Elektronenstrahlmikroskopie über die natürlichen Mischkristallbereiche der Skutterudite. *Contrib. Mineral. Petrol.* **11**, 322-333.
- \_\_\_\_\_, (1965b): Synthesen und Analysen in den Dreiecksdiagrammen FeAsS-CoAsS-NiAsS und FeS<sub>2</sub>-CoS<sub>2</sub>-NiS<sub>2</sub>. *Neues Jahrb. Mineral., Abh.* **103**, 205-255.
- KRETSCHMAR, U. & SCOTT, S.D. (1976): Phase relations involving arsenopyrite in the system Fe-As-S and their application. *Can. Mineral.* **14**, 364-386.
- MAUREL, C. & PICOT, P. (1974): Stabilité de l'allosclite et de la cobaltite dans les systèmes Co-As-S et Co-Ni-As-S. *Bull. Soc. Fr. Minéral. Cristallogr.* **97**, 251-256.
- MISRA, K. & FLEET, M.E. (1975): Textural and compositional variations in a Ni-Co-As assemblage. *Can. Mineral.* **13**, 8-14.
- MPOSKOS, E. (1983): A mineralogical study of the Au-Ag-Bi-Te-Cu-Co-Ni-As-S ore mineralization in Macedonia, Greece. *Chem. Erde* **42**, 281-296.
- NICKEL, E.H. (1970): The application of ligand-field concepts to an understanding of the structural stabilities and solid-solution limits of sulphides and related minerals. *Chem. Geol.* **5**, 233-241.
- OEN, I.S., BURKE, E.A.J., KIEFT, C. & WESTERHOF, A.B. (1971): Ni-arsenides, Ni-rich loellingite and (Fe,Co)-rich gersdorffite in Cr-Ni-ores from Malaga Province, Spain. *Neues Jahrb. Mineral., Abh.* **115**, 123-139.
- \_\_\_\_\_, DUNN, P.J. & KIEFT, C. (1984): The nickel-arsenide assemblage from Franklin, New Jersey: description and interpretation. *Neues Jahrb. Mineral., Abh.* **150**, 259-272.
- PERMINGEAT, F. & ZEHNI, A. (1988): La gersdorffite et la cobaltite des filons d'Oumjerane (Anti-Atlas oriental). *Notes Serv. Geol. Maroc* **44**, 249-251.
- PETRUK, W., HARRIS, D.C. & STEWART, J.M. (1971): Characteristics of the arsenides, sulfarsenides, and antimonides. *Can. Mineral.* **11**, 150-186.
- RADCLIFFE, D. & BERRY, L.G. (1968): The safflorite-löllingite solid solution series. *Am. Mineral.* **53**, 1856-1881.
- ROSEBOOM, E.H. (1962): Skutterudites (Co, Ni, Fe)As<sub>3-x</sub>: composition and cell dimensions. *Am. Mineral.* **47**, 310-327.
- \_\_\_\_\_, (1963): Co-Fe-Ni diarsenides: compositions and cell dimensions. *Am. Mineral.* **48**, 271-299.
- ROSNER, B. (1970): Untersuchungen mit der Elektronenstrahlmikroskopie an natürlichen Skutteruditen. *Contrib. Mineral. Petrol.* **28**, 135-146.
- SHARP, Z.D., ESSENE, E.J. & KELLY, W.C. (1985): A re-examination of the arsenopyrite geothermometer: pressure considerations and applications to natural assemblages. *Can. Mineral.* **23**, 517-534.
- SHENGELIA, D.M., AKHVLEDIANI, R.A. & KETSKHOVELI, D.N. (1977): The graphite geothermometer. *Dokl. Acad. Sci. USSR, Earth-Sci. Sect.* **235**, 132-134.
- SPIRIDONOV, E.M. & CHVILEVA, T.N. (1995): On the boundary between gersdorffite NiAsS and krutovite NiAs<sub>2</sub>. *Dokl. Acad. Sci. USSR, Earth-Sci. Sect.* **341**, 119-123.
- VINOGRADOVA, R.A., KRUTOV, G.A. & RUDASHEVSKIY, N.S. (1974): A variety of nickel allosclite. *Dokl. Akad. Nauk* **222**, 162-164 (in Russ.).
- WAGNER, T. & LORENZ, J. (2002): Mineralogy of complex Co-Ni-Bi vein mineralization, Bieber deposit, Spessart, Germany. *Mineral. Mag.* **66**, 385-407.
- YUND, R.A. (1962): The system Ni-As-S; phase relations and mineralogical significance. *Am. J. Sci.* **260**, 761-782.

Received January 29, 2004, revised manuscript accepted June 21, 2004.